iScience

Article

Chronic stress alters hepatic metabolism and thermodynamic respiratory efficiency affecting epigenetics in C57BL/6 mice

Chronic variable stress effect on hepatic metabolism
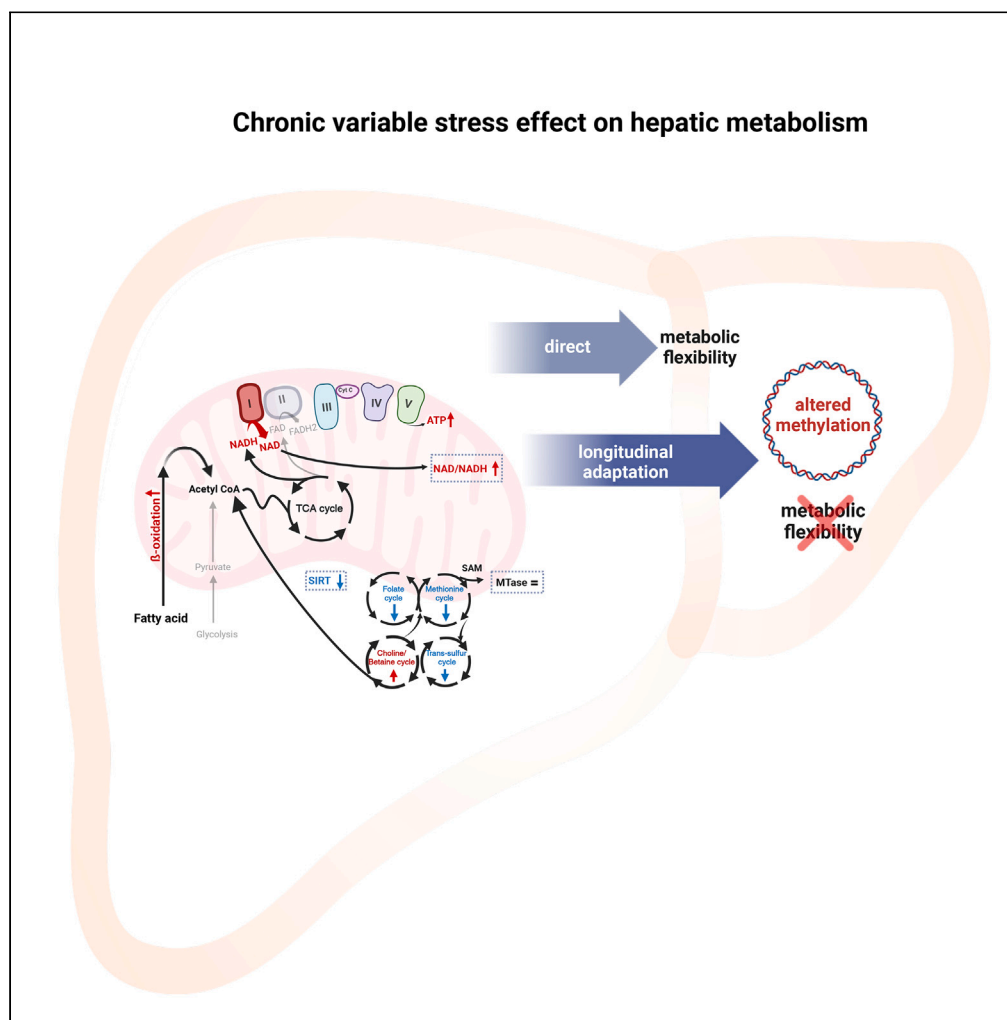
Aleksandra Nikolic, Pia Fahlbusch, Nele-Kathrien Riffelmann, ..., Hadi Al-Hasani, Jörg Kotzka, Birgit Knebel

birgit.knebel@ddz.de

Highlights

Chronic stress (Cvs) reduces the net energy utilization of supplied convertible energy

Cvs alters hepatic metabolism, affecting mitochondrial function and energy regulation

Cvs alters epigenetic pattern in mitochondrial DNA despite stress recovery

Reduced metabolic flexibility in hepatocytes is persistent after stress recovery

Article

Chronic stress alters hepatic metabolism and thermodynamic respiratory efficiency affecting epigenetics in C57BL/6 mice

Aleksandra Nikolic,[1,2,4] Pia Fahlbusch,[1,2,4] Nele-Kathrien Riffelmann,[1] Natalie Wahlers,[1] Sylvia Jacob,[1] Sonja Hartwig,[1,2] Ulrike Kettel,[1] Martina Schiller,[1] Matthias Dille,[1] Hadi Al-Hasani,[1,2,3] Jörg Kotzka,[1,2,5] and Birgit Knebel[1,2,5,6,*]

SUMMARY

Chronic stress episodes increase metabolic disease risk even after recovery. We propose that persistent stress detrimentally impacts hepatic metabolic reprogramming, particularly mitochondrial function. In male C57BL/6 mice chronic variable stress (Cvs) reduced energy expenditure (EE) and body mass despite increased energy intake versus controls. This coincided with decreased glucose metabolism and increased lipid β-oxidation, correlating with EE. After Cvs, mitochondrial function revealed increased thermodynamic efficiency (η-opt) of complex CI, positively correlating with blood glucose and NEFA and inversely with EE. After Cvs recovery, the metabolic flexibility of hepatocytes was lost. Reduced CI-driving NAD+/NADH ratio, and diminished methylation-related one-carbon cycle components hinted at epigenetic regulation. Although initial DNA methylation differences were minimal after Cvs, they diverged during the recovery phase. Here, the altered enrichment of mitochondrial DNA methylation and linked transcriptional networks were observed. In conclusion, Cvs rapidly initiates the reprogramming of hepatic energy metabolism, supported by lasting epigenetic modifications.

INTRODUCTION

The prevalence of metabolically related disorders including insulin resistance, glucose intolerance, obesity, dyslipidemia, and metabolically associated fatty liver disease (MAFLD; former non-alcoholic fatty liver disease (NAFLD)) is increasing globally. While factors such as genetics, overnutrition, and physical inactivity partially explain this trend, the stress of modern life may contribute to the overall risk. Studies have shown that individuals with stress-related disorders are at higher risk of developing these disorders, even after a stress-free recovery period.[1–5] This suggests that stress has long-term effects on metabolism.

An established response to an altered environment is a change in epigenetics, specifically in 5-methylcytosine (^{met}C) patterns, that can act as a memory to maintain altered gene expression without changes in DNA sequence.[6] This concept is well-established in early life metabolic programming, nutrient disposition, and transgenerational transmission of metabolic risk.[7–9] Research links epigenetics to metabolic syndrome through associations with relevant traits and metabolic stress in mice and men.[10–14]

Previous investigations on the epigenetics of chronic stress have mainly focused on neurological and neurophysiological aspects, but also provide evidence that various chronic and acute stress exposure directly targeted mitochondria, especially in neurological tissues.[15–17] However, limited information is available regarding the impact of stress on energy metabolism in the liver.[18] The liver is highly dependent on mitochondria functionality, particularly to meet the energy requirements for maintaining hepatic metabolism and also whole-body energy expenditure (EE).[19]

Acute stress response increases energy demands met by ATP and energy equivalents generated by mitochondrial oxidative phosphorylation. Key metabolic pathways as fatty acid oxidation (FAO), tricarboxylic acid cycle (TCA), or one-carbon cycle (OCM) are compartmentalized within mitochondria,[20–22] also providing signaling metabolites and methylation donors for regulatory processes including DNA methylation.[8,22] At least, impaired mitochondrial function is associated with metabolic disorders such as obesity, type 2 diabetes, and MAFLD.[23–25]

We have previously shown that chronic stress leads to hepatic insulin resistance and increased triglyceride levels after 3-month recovery.[26] To this time, the liver further undergoes metabolic adaptations during stress recovery, resulting in altered blood glucose levels, glucose
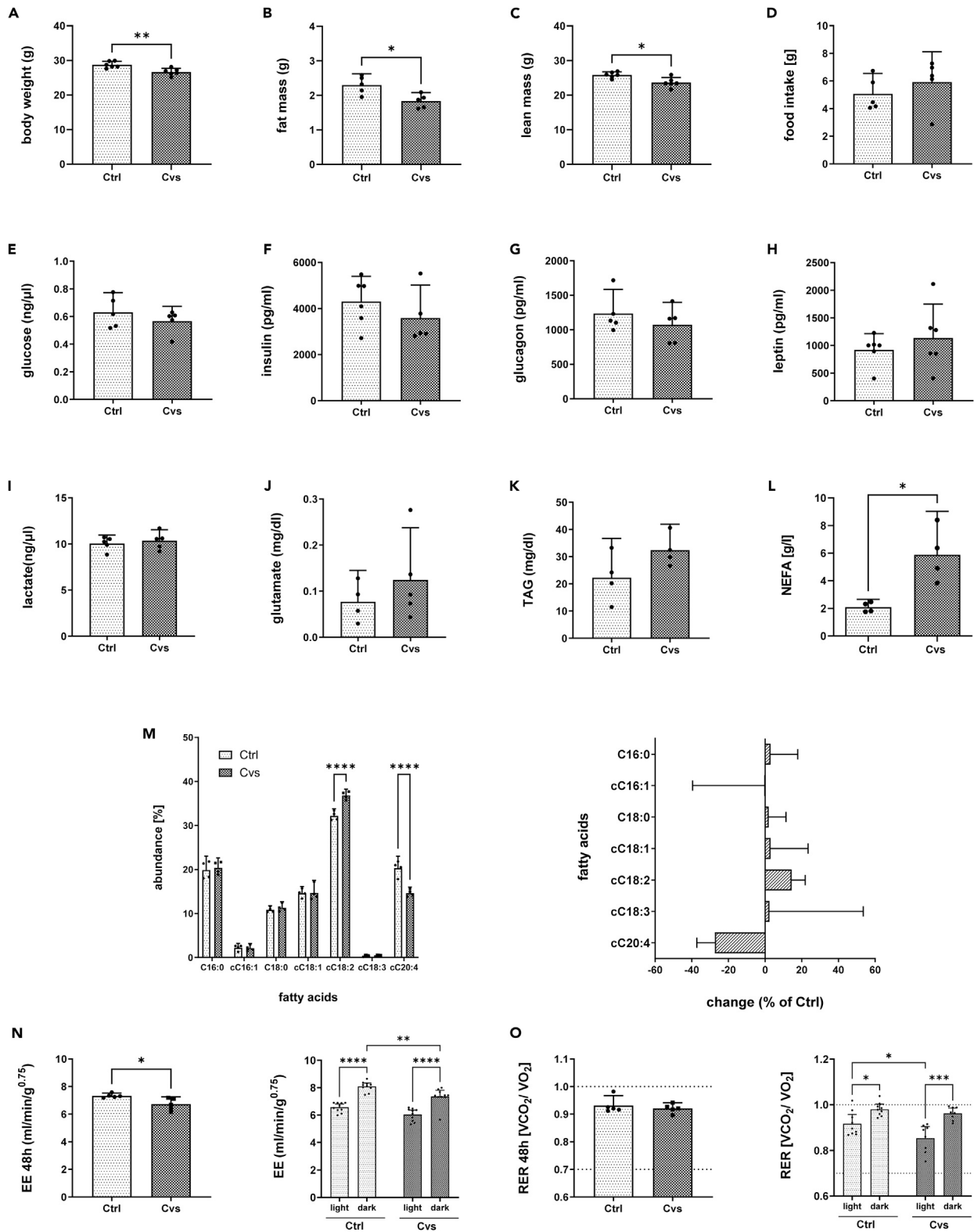
Figure 1. Systemic effects of a 15-day chronic stress intervention (Cvs)

(A) body weight, (B) fat mass, (C) lean mass, in control (Ctrl) and Cvs (n = 5–6/group).

(D) Differences in food intake during Cvs intervention are shown per group (n = 6/group). Intermediate substrate levels of (E) glucose, (F) insulin, (G) glucagon, (H) leptin, (I) lactate, (J) glutamate, (K) TAG, (L) NEFA in plasma after Cvs compared to Ctrl group.

(M) Plasma NEFA composition. Mean values of percentage distribution are shown, with the sum of measurements set to 100%. Asterisks indicate significant changes in fatty acid content (p < 0.01).

(N) Indirect calorimetry with total energy expenditure (EE) and (O) respiratory exchange ratio (RER) Indirect calorimetry data are given over 48h or the combined results of light and dark phases are reported individually. Bar graphs represent the mean ± 95% CI (n = 4–6/group). Individual measurements are shown as dots. Statistics: Mann-Whitney test or one-way ANOVA with Tukey test for multiple comparisons, *p < 0.05, **p < 0.01, ***p < 0.001, ****p < 0.0001, Ctrl: C57BL/6, Cvs: C57BL/6 after stress intervention. The dashed lines in the RER plot (O) mark the thresholds for preferential carbohydrate oxidation (VCO_2/VO_2 = 1.0) or lipid oxidation (VCO_2/VO_2 = 0.7).

tolerance, hepatic triglycerides, lipogenesis, lipid uptake, and FAO.[27] NAD^+ levels are reduced directly after stress and SIRT activity longitudinal after stress,[27] indicating a potential influence of stress on epigenetic mechanisms of gene regulation.

Based on this background, the aim of our study was to investigate the immediate effects of chronic variable stress (Cvs) on the liver, exploring molecular mechanisms and sustainable consequences on epigenetics. We assessed the acute effects of stress using indirect calorimetry, blood tests, proteomics and functional assays. We examined the effects of stress on mitochondrial complexes, focusing on their activity and thermodynamic efficiency. Epigenetic and transcriptomic analyses were performed immediately after stress and after a recovery period.

Overall, our study provides insights into the immediate effects of chronic stress on the liver and elucidates the underlying molecular mechanisms. These findings contribute to our understanding of the long-term consequences of chronic stress on metabolism and highlight the importance of mitochondrial function in maintaining energy homeostasis.

RESULTS

Chronic variable stress interferes with hepatic metabolism

Immediately after undergoing our stress protocol, stressed C57BL/6 mice (Cvs) or untreated littermates (Ctrl) were tested for acute metabolic effects. Cvs mice exhibited a significant decrease in body weight (6.2%), fat mass (21%), and lean mass (8.1%) (Figures 1A–1C) compared to the Ctrl mice, despite unchanged food intake (Figure 1D). Insulin resistance and dysfunctional gluconeogenesis was excluded (Figures S1A and S1B). Of plasma parameters analyzed (Figures 1E–1K), solely non-esterified fatty acid (NEFA) levels were three times higher in Cvs mice than in Ctrl mice (Figure 1L), with increased linoleic acid (cC18:2) (14.6%) and decreased arachidonic acid (cC20:4) (27.7%) levels after Cvs compared to Ctrl (Figure 1M). Diurnal metabolic capacity was assessed by indirect calorimetry to distinguish between low (light) and high (dark) activity levels. Total EE throughout the observation period was significantly lower after Cvs compared to Ctrl (Cvs: 6.7 mL/min/g^{075}; Ctrl: 7.3 mL/min/g^{075}), especially during the dark phase (Ctrl: 8.0 mL/min/g^{075}; Cvs: 7.3 mL/min/g^{075}) (Figure 1N). Furthermore, correlation analyses between plasma parameters and light and dark EE showed a significant relationship between dark EE and plasma NEFA (dark: R^2 = 0.5491; p = 0.0354), especially cC18:2 (dark: R^2 = 0.6574; p = 0.0146) after Cvs. The respiratory exchange ratio (RER) remained unchanged after Cvs (Figure 1O). Diurnally, RER was higher in the dark phase (Ctrl: +7.7%; Cvs: +13%) in both groups compared to the light phase. In stressed animals, RER was significantly decreased by 6.5% in the light phase (Ctrl: 0.91 mg/min; Cvs: 0.85 mg/min) compared with control mice (Figure 1O), supported by reduced NAD^+ dependent cytosolic SIRT activity as a metabolic sensor for redox states (Figure S1C). NEFAs correlated with RER, particularly light phase RER (light: R^2 = 0.5083; p = 0.0471), and cC18:2 (light: R^2 = 0.5136; p = 0.0455) after Cvs.

Altered protein abundance and functionality in main pathways for glucose and lipid metabolism after chronic variable stress

To investigate the immediate impact of the stress intervention on metabolic pathways, a label-free proteomic analysis was performed on the hepatic 11,000xg protein fraction to assess the status quo of protein content in Cvs liver. In addition, enzyme activity assays of key pathways related to glucose and lipid metabolism were conducted *ex vivo* on isolated hepatocytes. Proteomic analyses revealed 3222 differentially abundant proteins. At 1.5-fold regulation 29 up-regulated and 91 down-regulated proteins were identified by Student's *t* test (p < 0.05) (Table S1). GO analysis revealed the up-regulation of catabolic processes and a down-regulation of anabolic processes immediately after stress (Table S1).

The abundance of detected proteins involved in the glycolysis pathway was significantly reduced (p < 0.0001). Consistent with this, the glucose-stimulated rate of glycolysis was 39% lower immediately after stress (Figure 2A). Proteins involved in ketone metabolism were enriched in Cvs (p < 0.05), but hepatic β-hydroxybutyrate concentrations immediately after Cvs were not altered (Figure 2B). Proteins involved in gluconeogenesis were less abundant after stress (p < 0.0001). Although basal rates of hepatocyte gluconeogenesis were 2-fold higher, the ability to achieve substrate-stimulated glucose secretion was reduced in the Cvs compared to the Ctrl group. The suppression of gluconeogenesis by insulin administration was also reduced in hepatocytes (Figure 2C). Interestingly, the hepatic glucose level, reflecting glucose homeostasis in the liver, was unaltered immediately after stress (Figure 2D).

Regarding the immediate stress effects on lipid metabolism, Cvs decreased the abundance of DNL associated proteins (p < 0.0001), but hepatocyte DNL activity was yet unaltered between the groups (Figure 2E). Cvs did not affect the abundance of proteins involved in triglyceride synthesis/lipid droplet formation, and hepatic TG content (Figure 2F). In contrast, protein abundance of the mitochondrial β-oxidation pathway was significantly increased (p < 0.0001), which was accompanied by a 6-fold increase in mitochondrial β-oxidation activity after Cvs in hepatocytes (Figure 2G). After Cvs, proteins of the one carbon-metabolism (OCM), providing and recycling methyl donors, were decreased in

Figure 2. Cvs intervention impairs hepatic protein abundance and *ex vivo* activity of key metabolic pathways

Proteomic data and the respective *ex vivo* metabolic activities shown as bar graphs in primary hepatocytes from Ctrl and Cvs.

(A) Glycolysis, (B) ketone metabolism, (C) gluconeogenesis, (D) glucose level in liver tissue, (E) *de novo* lipogenesis (F) TG synthesis/lipid droplet formation and hepatic TG content, (G) mitochondrial β-oxidation, and (H) protein abundance of one-carbon metabolism. *Z* score plots show the over- and underrepresentation of proteins associated with the indicated signaling pathways from a label-free proteome analysis of the liver 11,000 xg fraction. Red represents up-regulation, blue represents down-regulation, and white represents no change in protein abundance of the mean of each condition relative to the overall mean of the experiment. The corresponding estimation plots show the mean values for each protein (dots) and the mean change in the pathway of the Cvs and Ctrl group ±95% CI. The left axis shows the mean *Z* score and the right axis shows the effect size (n = 5/group). Statistics: Mann-Whitney test or one-way ANOVA with Tukey test for multiple comparisons, **p < 0.01, ***p < 0.001, ****p < 0.0001, Ctrl: C57BL/6, Cvs: C57BL/6 after stress intervention. Proteome analysis (n = 5/group), activity assays in hepatocytes (n = 6/group). Dots in bar graphs represent individual measurements. TG: triglyceride, FA: fatty acid, Pyr/Lac: pyruvate/lactate, eto: etoxomir.

the methionine, folic acid, and *trans*-sulfur cycles and increased in the choline/betaine cycle compared to Ctrl (Figure 2H); but activities of methyltransferases were unaltered (Figure S1D). Furthermore, a correlation between the β-oxidation rate and dark phase EE (dark: R^2 = 0.5996; p = 0.0410) was observed, highlighting the immediate effect of the stress intervention on mitochondrial function.

Chronic variable stress interferes with mitochondrial function in liver

Cvs did not alter the mitochondrial DNA amount, membrane integrity based on cytochrome-*c*-oxidase activity, or mitochondrial content determined by the commonly used validated biomarker citrate synthase activity[28,29] (Figure S2A). The abundance of redox-regulating proteins was decreased after Cvs (p < 0.0001), with enzyme analysis indicating unchanged redox balance in Cvs compared to Ctrl (Figure S2B). However, the mitochondrial protein composition showed that the differential abundance of the electron transport chain (ETC) proteins resulted in a significant increase in the components of complexes (C) I (p < 0.0001), CII (p = 0.0279), CIII (p < 0.0001), CIV (p = 0.0474) and CV (p < 0.0001) after Cvs compared to Ctrl (Figure 3A). In addition, the mitochondrial electron flow capacity was functional in the uncoupled state without substrate limitation. It was unaltered via CI and even increased via CII after Cvs compared to Ctrl. CIV activity also showed enhanced function after Cvs compared to Ctrl when directly targeted by the electron donor TMPD (Figure 3B).

Therefore, further analysis of mitochondrial function focused on the coupling efficiency through either CI or CII of the (ETC) to ATP synthase (CV) were performed. Respiration data were normalized by defined protein input and by the accepted mitochondrial content marker citrate synthase activity.[29–32] The combination of these two normalization strategies were used to avoid possible normalization-related misinterpretations. So, the Cvs effects presented are therefore independent of potential alterations in the total protein content of the enriched fractions or the amount of mitochondria based on citrate synthase activity We measured basal OCR and the electron transport capacity with complex-specific substrate limitation in enriched liver mitochondria, with the simultaneous inhibition of the respective other complex using either malonate or rotenone in two different experimental setups (Figures 4A and 4B). CI-driven respiration was forced by pyruvate/malate and concomitant inhibition of CII by malonate (Figure 4A). Detailed examination of CI-driven oxygen consumption (states 2, 3, 3u, 4o) and calculated measures of oxidative phosphorylation, i.e., ACR and RCR (Figures S3A–S3E), revealed significantly increased OCR in state3u by 21% in Cvs compared to Ctrl (Figure S3C), whereas CII-specific coupling was not affected by Cvs (Figures S3F–S3J).

For detailed bioenergetic evaluation we calculated thermodynamic coupling degrees, i.e., q-values, applying thresholds for maximum net output current (ATP) at optimal efficiency (q_f = 0.786), maximum net output power ($q\rho$ = 0.910), net economic output current (q_f^{ec} = 0.953), and net economic output power at optimal efficiency ($q\rho^{ec}$ = 0.972).[33] In enriched mitochondria with controlled substrate delivery maximal net ATP output was achieved at optimal efficiency (> qf (=0.786)) in Ctrl animals, whereas the q-value was increased to a maximal net output (>qρ (=0.910)) in the stressed animals (Figure 4C). Ctrl mice reached the maximum net output thermodynamic coupling (<qρ (=0.910)), and Cvs mice approached the net economic output (<qf^{ec} (=0.953)) for CII (Figure 4C). Correspondingly, thermodynamic efficiency of substrate-to-energy conversion (*η-opt*) related to thermodynamic coupling showed a significant 2-fold increase in Cvs mitochondria specific to CI compared to the Ctrl, but remained unchanged for CII (Figure 4D). The *η-opt* of CI correlated negatively with dark EE (dark: R^2 = 0.6852; p < 0.01) and positively with plasma NEFA (R^2 = 0.7978; p < 0.01) after Cvs in contrast to Ctrl. The cellular NAD$^+$/NADH ratio linked to CI activity was significantly 3-fold higher (p = 0.0079) compared to Ctrl (Figure 4E), while FAD$^+$ tied to CII remained unchanged (Figure 4F).

Considering the hepatic metabolic memory after Cvs,[27] the energetic phenotype was assessed acutely after Cvs and in a separate group of mice who received a three-month recovery phase by plotting mitochondrial OCR versus ECAR in primary hepatocytes (Figure 4I). Comparison of hepatocytes from *acuteCvs* and *acuteCtrl* exhibit similar basal and uncoupled energy phenotypes, the latter defining the maximal respiratory capacity, which allows obtaining a reference state of reduced mitochondrial membrane potential. However, after recovery, the uncoupling of hepatocytes derived from *recoveryCvs* remains at basal energy states, while hepatocytes from the *recoveryCtrl* still show a shift toward an energetic phenotype. These results indicate a long-term loss of metabolic flexibility in hepatocytes from Cvs animals.

The molecular action of stress interferes with gene regulation in two phases

Apart from energy metabolism, mitochondria are an important mediator of signal transduction, genetic and epigenetic processes. To explore the potential association between acute stress exposure and long-term metabolic effects, we performed an analysis of hepatic methylation and transcription patterns at two time-points. First, we compared the patterns immediately after the stress phase between the acute control group and the acute stress intervention group (direct comparison: *acuteCtrl* vs. *acuteCvs*). Second, we evaluated the individual progression in a separate group of mice who received a three-month recovery period after the chronic stress intervention (longitudinal comparison: *acuteCtrl* vs. *recoveryCtrl* and *acuteCvs* vs. *recoveryCvs*, respectively) (Figure 5). The methylation and transcriptional analyses revealed that the variability after facing Cvs was reduced over time compared to the longitudinal progression of the unstressed littermates (Figures 5A and 5B). There was no accumulation in specific genomic regions (Figure 5C). The genomic architecture of the mouse genome differs from the human genome, but the gene regulatory promoter organization and epigenetic interference with transcription factor binding sites is comparable to humans. Therefore, we further focused our analyses on the evaluation of genes with methylation in the core promoters (≤-3kb to TSS) (Figure 5D). This indicated an accumulation of differential methylation especially on mitochondrial DNA in the longitudinal observation after Cvs (Figure 5D).

Effect of stress on the methylome

In detail, the correlation of all methylation datasets (*acuteCtrl*, *acuteCvs*, *recoveryCtrl*, or *recoveryCvs*) was high, indicating limited overall stress impact (Table S2). Comparing the acute conditions, differences in enriched methylated fragments within *acuteCtrl* and *acuteCvs*
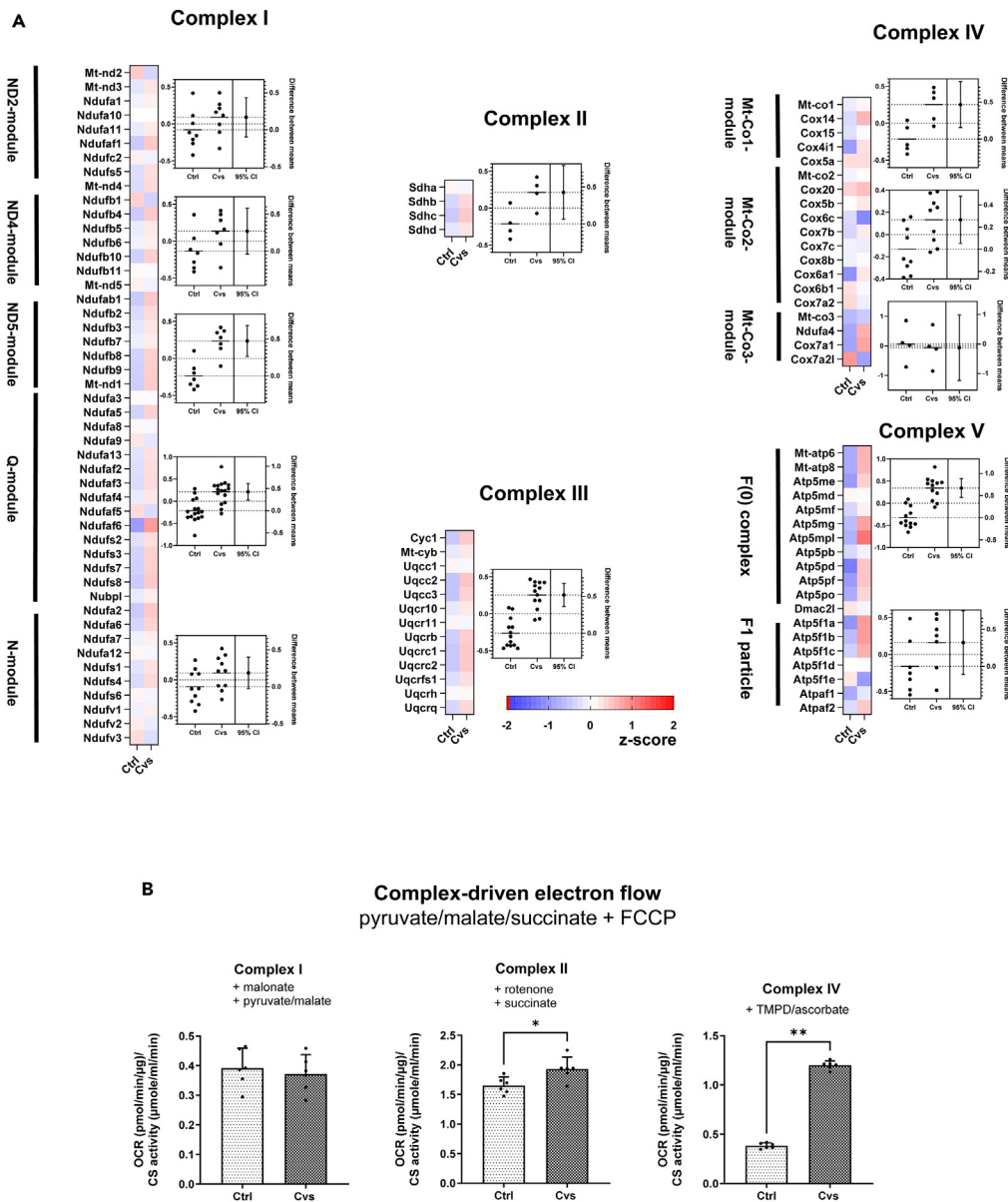
Figure 3. Mitochondrial proteome and electron flow assessment

(A) Heat maps resulting from Z score analyses and estimation plots of protein abundance for individual complex (C)I, II, III, IV, and V subunits of the electron transport chain. Red indicates up-regulation, and blue indicates the down-regulation of proteins. White indicates no change.

(B) Electron flow measured in the 11.000xg fraction at uncoupled state of the mitochondrial membrane. The oxygen consumption rate (OCR) in relation to citrate synthase activity (CS) is shown. Data were normalized to total protein content and citrate synthase activity. Injection strategies: CI: stimulation with pyruvate and malate after the malonate inhibition of CII; CII: stimulation with succinate after the rotenone inhibition of CI; CIV: stimulation by TMPD/ascorbate after Antimycin A inhibition of CIII. Ctrl: C57BL/6, Cvs: C57BL/6 after stress intervention. Data are expressed as mean ± 95% CI (n = 6/group). Individual measurements are shown as dots. Statistics: Mann-Whitney test or one-way ANOVA with Tukey test for multiple comparisons, *p < 0.05.

indicated that enriched fragments showed 98.2% (99.1% if within primary promoters) overrepresentation of methylation in *acuteCvs*. 170 significant chromosomal frames showed overrepresented methylation in *acuteCvs*, including 5 promoter regions of known genes, i.e., Trav23 or Cdc14b. In addition, 4 chromosomal frames showed overrepresented methylation in *acuteCtrl* compared to *acuteCvs*, including the mt-Nd6 promoter region (<1kb) of with an edgR-fold change of 0.4–0.57 (edgRp-value $2.69E^{-07} - 4.28E^{-16}$). GO analyses revealed no significant enriched pathway from these findings (Table S2). In the longitudinal observation of Ctrl, 99.7% (99.3% if within primary promoters), of fragments showed methylation overrepresentation. Here, 9 chromosomal regions were more methylated in *acuteCtrl* than in *recoveryCtrl*, including promoters of serpinf-1 and various unknown genes. Vice versa, 796 significant frames including frames covering promoters of 50 annotated genes
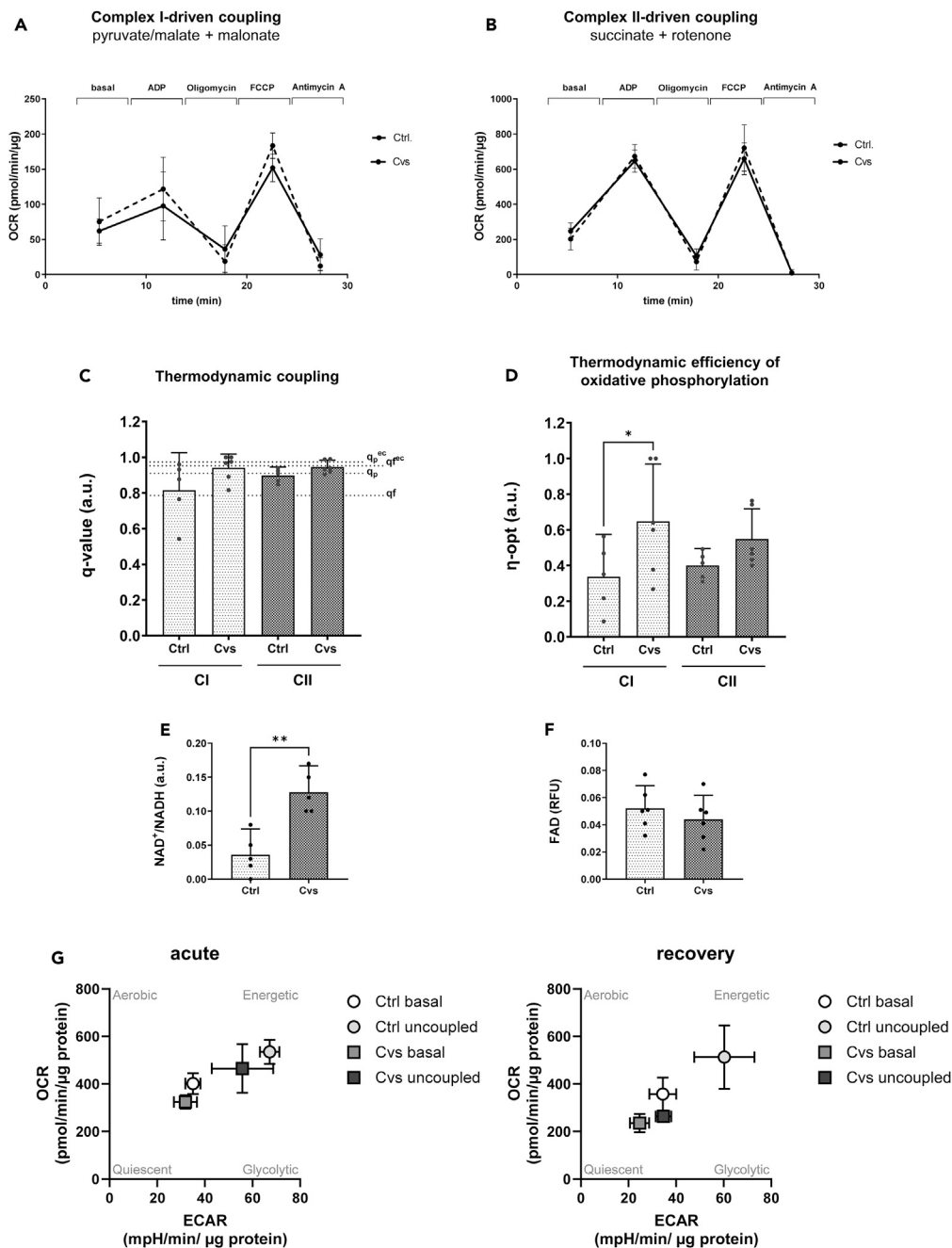
Figure 4. Mitochondrial complex I efficiency is increased after CVS

Mitochondrial coupling efficiency, thermodynamic coupling and thermodynamic efficiency of oxidative phosphorylation specific for ETC complex CI and CII were studied in mitochondria-enriched fractions (11,000xg fractions). Experiments were performed specifically for CI- and CII-driven mitochondrial coupling by the measurement of the oxygen consumption rate (OCR).

(A) Complex I-specific OCR (CI stimulation: pyruvate and malate, simultaneous CII inhibition: malonate). CII-specific OCR (CII stimulation: succinate, simultaneous CI inhibition: rotenone).

(B) Mitochondrial respiration determined at basal and at the serial injection of ADP, oligomycin, FCCP, and Antimycin A. Data points represent the mean of n = 5–6 animals/group shown as mean $\pm$ 95% CI. Detailed data interpretations are given in Figure S4.

(C) Thermodynamic coupling q-values, and (D) thermodynamic efficiency (η-opt) of oxidative phosphorylation calculated for CI- and CII-specific respiration. Dotted lines: maximal coupling values of thermodynamic thresholds corresponding to maximal net output flow (ATP) at optimal efficiency (qf = 0.786), maximal net output power (qp = 0.910), economic net output flow (qf^{ec} = 0.953), and economic net output power at optimal efficiency (qp^{ec} = 0.972). Data points represent the mean of n = 5 animals/group shown as mean $\pm$ 95% CI.

Figure 4. Continued

(E) NAD$^+$/NADH ratio, (F) FAD$^+$ abundance. Data points represent the mean of n = 4–6 animals/group shown as mean ± 95% CI.

(G) Mitochondrial energy phenotype immediately after Cvs (acute) and after 3-month recovery (recovery) compared to age-matched controls in primary hepatocytes culture at basal and uncoupled conditions. Energetic phenotype was assessed by plotting OCR vs. ECAR (n = 6/group). All OCR values were normalized by citrate synthase activity to adjust for mitochondrial content. Ctrl: C57BL/6, Cvs: C57BL/6 after stress intervention. Individual measurements are shown as dots. Statistics: Mann-Whitney test or one-way ANOVA with Tukey test for multiple comparisons, *p < 0.05, **p < 0.01.

showed overrerepresented methylation in *recoveryCtrl*. These included Trav23 and eight mitochondrial-coded genes, i.e.,: mt-Tt, mt-Ts, mt-Tw, mt-Atp6, mt-Nd5, mt-Nd3, mt-Nd6, and mt-Rn2 (Table S2). Focusing on core promoter methylated genes, GO analyses did not reach FDR significance (Table S2). In contrast, in the longitudinal comparison of Cvs animals 90% of all enriched fragments showed methylation over-representation after recovery. Within primary promoters, methylation dropped to 84% after recovery. There were 82 chromosomal regions with more methylation in *acuteCvs*. When targeting promoter regions, these were mainly uncharacterized genes. 593 chromosomal frames showed overrepresented methylation in *recoveryCvs*. Focusing on promoter methylation, further these included 16 mitochondrial-coded genes, i.e., mt-Atp6, mt-Co1, mt-Nd1, mt-Nd2, mt-Nd4, mt-Nd5, mt-Nd6, mt-Rnr2, mt-Th, mt-Tl1, mt-Tp, mt-Tr, mt-Ts1, mt-Tt, mt-Tv, and mt-Tw. Notably, only three frames covered identical mitochondrial regions in Ctrl and Cvs, all others were specific to either longitudinal analysis. Of all conditions analyzed a significant enrichment of pathways, was solely observed for genes methylated in primary promoters in the longitudinal Cvs analyses. Here, various aspects of mitochondrial ATP synthesis related to electron transport were significantly enriched (enrichment p value 3.71E^{-09}, FDR 9.74E^{-06}) (Table S2).

Effect of stress on the transcriptome

Directly after Cvs, gene expression analysis identified 859 differentially regulated functionally annotated molecules, with 553 up in Ctrl and 305 up in Cvs (Figure 4B, Table S3). The molecules were associated with lipid metabolic pathways, such as cholesterol biosynthesis and reduced triacylglycerol biosynthesis (Table S3). Enrichment in central hepatic signaling pathways related to nuclear receptor RXR function or hetero-dimerization, type 2 diabetes mellitus, and hepatic fibrosis-related signaling was observed (Table S3). Pathways related to mitochondrial function and redox systems, including NRF2-mediated oxidative stress response, sirtuin signaling, glutathione-mediated detoxification, mito-chondrial L-carnitine shuttle or NAD$^+$ signaling pathway were also differentially enriched (Table S3). In the longitudinal analyses of Ctrl animals, 1401 genes showed differential abundance with 716 up in *acuteCtrl*, and 738 in *recoveryCtrl* (Table S3). Here, various signaling path-ways including PPARα/RXRα activation, mTOR, PI3K/AKT, or glucocorticoid signaling were affected. Metabolic pathways including choles-terol-, and triacylglycerol biosynthesis, apoptosis, inflammatory signaling, as well as DNA methylation or transcriptional repression signaling, showed differential abundance. About mitochondrial function, sirtuin, EIF2 and NAD$^+$-signaling, and oxidative phosphorylation, showed dif-ferential abundance in the longitudinal observation of Ctrl (Table S3). In the longitudinal analyses of Cvs, consistent with the reduced tran-scriptional variability after Cvs, 210 genes are less abundant in *acuteCvs*, and 710 were more abundant in *recoveryCvs*. Enrichment of gluco-corticoid receptor signaling molecules was higher in the longitudinal Cvs than in longitudinal Ctrl observation and affects different molecules. Furthermore, metabolic pathways such as cholesterol biosynthesis, and pathways regulated by various nuclear receptor complexes and gly-colyisi related transcripts were differentially regulated (Table S3). Regarding mitochondrial function the differential regulation of transcripts annotated to mitochondrial dysfunction, oxidative phosphorylation, NAD$^+$-signaling, sirtuin signaling, or NRF2-mediated oxidative stress response predicted differential activity. Interestingly, no enrichment in lipid biosynthetic pathways was detected in the longitudinal observa-tion after previous Cvs. Of note, transcription differences were specific to either longitudinal analysis.

So, the longitudinal observation indicated that mitochondrial DNA methylation showed different patterns depending on whether animals were exposed to acute stress (Figure 6A). From the methylation and transcription data, it can be inferred that Cvs had a longitudinal effect on mt-DNA methylation and on transcriptional regulation (Figure 6B).

DISCUSSION

Chronic stress is associated with the development of diabetes, metabolic disorders, and fatty liver disease, affecting energy metabolism and mitochondrial function. In previous studies in our Cvs mouse model, we found that chronic stress had immediate tissue-specific effects, with subsequent metabolic adaptations leading to increased hepatic lipid accumulation even after stress-free recovery.[26,27] In this study, we hy-pothesized that the molecular basis of the increased metabolic risk is implemented immediately after Cvs in the liver leading to the long term adaptation of metabolism even after stress-free recovery. Our findings revealed that immediately following chronic stress: (i) reduced meta-bolic capacity, evident through decreased EE and RER correlated with circulating NEFAs, especially linoleic acid (cC18:2); (ii) changes in the hepatic proteome indicating reduced glucose metabolism and increased lipid catabolism, confirmed by metabolic activity analyses; (iii) altered abundance of oxidative phosphorylation components, not affecting electron flow capacity but increasing mitochondrial thermody-namic efficiency of CI; (iv) epigenetic modifications, not directly explaining the observed acute differential gene expression. However, observing stressed mice over time, we identified distinct epigenetic patterns different from unstressed mice especially in mtDNA. Here, differ-entces in mtDNA methylation, are accompanied by corresponding effects on mitochondrial transcriptional networks.

Analyzing chronic stress in a standardized preclinical model allows us to study the effects of cellular adaptations on maintaining energy balance, minimizing confounding factors present in more complex clinical studies. Our model accurately reflects the effects of corticosterone on insulin-responsive tissues, mimicking the risk of metabolic syndrome associated with stress and glucocorticoid exposure in
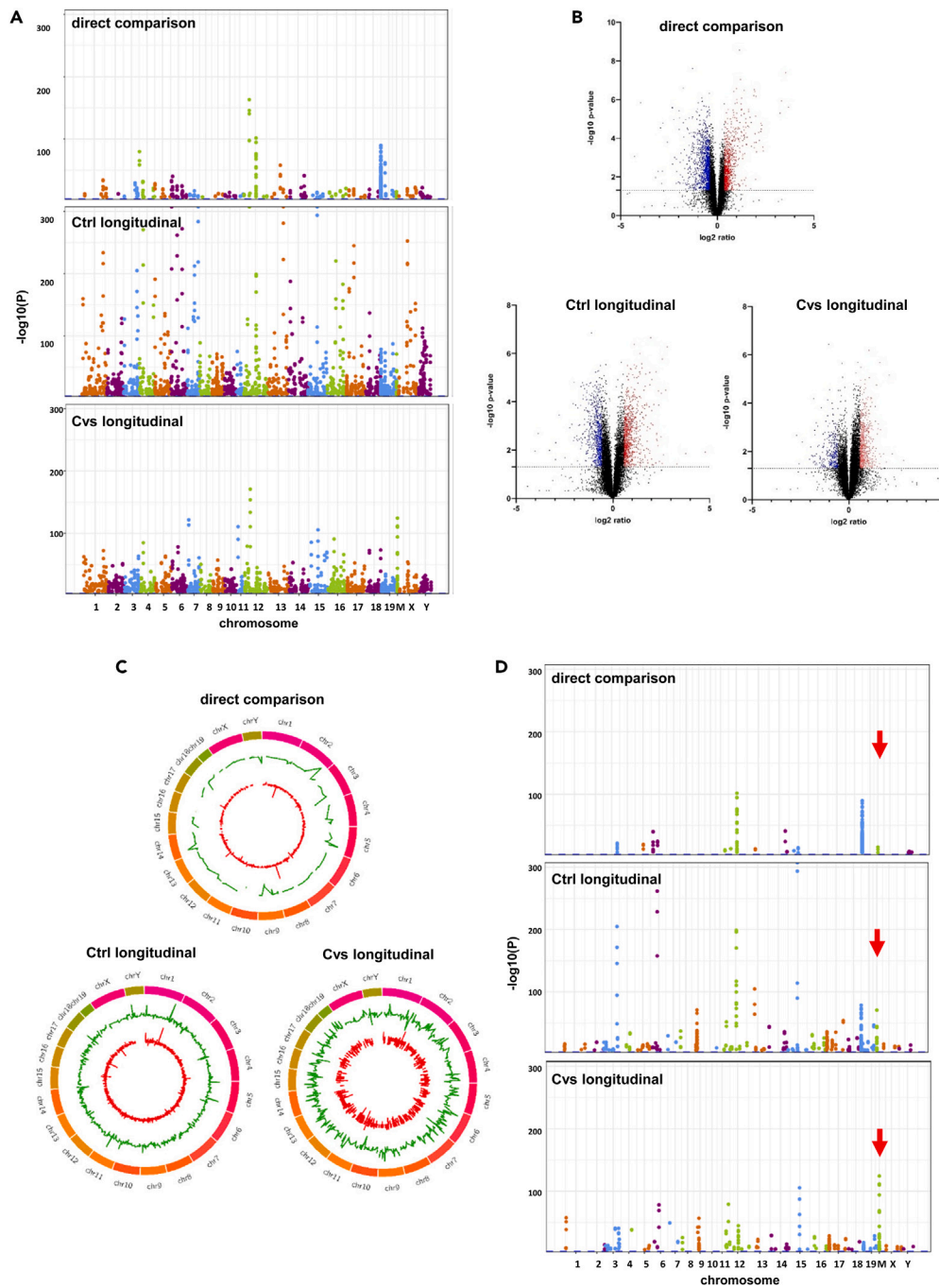
Figure 5. Molecular action of stress on hepatic genetic and epigenetic processes

Methylation and transcriptional differences in the liver were analyzed immediately after Cvs (direct comparison: *acuteCtrl* vs. *acuteCvs*) or after 3-month recovery (longitudinal of either Ctrl or Cvs: *acute* vs. *recovery*).

(A) Manhattan plot (y axis: -log10 p-value; x axis: chromosomal localization) of all differentially methylated fragments based on edgeR.p.value (Supplement Methylation; n = 3–5/condition).

(B) Volcano plot analyses (y axis: -log10 p-value; x axis: log2 fold ratio) of all differentially transcribed genes. Color code: blue; enriched in condition 1 (direct comparison: *acuteCtrl*; Ctrl longitudinal: *acuteCtrl*; Cvs longitudinal: *acuteCvs*)) red enriched in condition 2 (direct comparison: *acuteCvs*; Ctrl longitudinal: *recoveryCtrl*; Cvs longitudinal: *recoveryCvs*) (Supplement Transcription; n = 5/condition).

(C) Circus plot analyses for genomic overview of differentially methylated fragments and differential transcription. Inner circle (red stacked histogram): transcriptome data (*acuteCtrl* vs. *acuteCvs*; *acuteCtrl* vs. *recoveryCtrl*; *acuteCvs* vs. *recoveryCvs*), outer circle (green line) methylome data (*acuteCtrl* vs.

humans.[4,26,27,34–37] After acute Cvs, our previous analyses showed a shift to FAO for whole-body energy generation, accompanied by increased lipolysis to compensate for EE under identical feeding conditions.[38] This was supported by a recent study, also determining FAO as a major source of energy in a Cvs-like model.[39] Next to increased serum NEFAs, we here noted changes in serum fatty acid patterns with increased linoleic acid (cC18:2) and decreased arachidonic acid (cC20:4) levels following stress. NEFA and linoleic acid levels correlated with the activity phase EE, suggesting that linoleic acid may undergo direct β-oxidation immediately after Cvs for energy supply. Linoleic acid responds to increased energy demand by localizing to mitochondria, influencing lipid metabolism genes, especially carnitine acyltransferases (CPTs) controlling mitochondrial fatty acid uptake.[40] In stressed mice, CPT2 expression is minimally regulated, while CPT1A increases, suggesting enhanced mitochondrial fatty acid uptake. The reduced arachidonic acid in our study aligns with the absence of inflammation in our Cvs model.[27] So, the model reflects severe stress in humans regarding increased beta-oxidation with decreased essential and long-chain fatty acids but does not show increased inflammation.[3–5] The elevated cC18:2 levels observed in our study are in line with those in NAFLD.[41] We previously found an increase in liver fat after the recovery phase in our Cvs model, but not acutely following stress.[27] The gene expression data indicate suppressed lipid synthesis during the longitudinal observation of Cvs. DNL activity immediately after stress is consistent with previous chronic, intermittent, or social defeat stress in animal studies and human PTSD.[4,5,42,43] However, in contrast to those studies, we observed increased FAO in our model in liver. Based on our data, one possible explanation for this discrepancy could be the attempt to supply energy for a more efficient oxidative phosphorylation in our model after acute stress.

The glucose-fatty acid cycle plays a crucial role in fuel metabolism.[44] Immediately after Cvs, stressed mice show decreased hepatic glucose metabolism, with suppressed hepatic glycolysis and gluconeogenesis pathways in proteome and functional data. The key enzyme G6P is repressed at transcription and protein levels and especially in the longitudinal transcriptional analyses of Cvs after stress recovery, no lipid synthesis genes are regulated and glycolysis-related transcription is reduced. So, Cvs differs from glucocorticoid action, as glucocorticoid excess increases hepatic glucose production by directly inducing G6P for gluconeogenesis in patients with Cushing syndrome.[45] NEFAs transported to the liver following Cvs further reduce glucose metabolism. Immediately after Cvs DNL decreased, ketogenesis remained unaffected, and mitochondrial β-oxidation increased. However, stable levels of hepatic glucose and DNL-derived cC16:1 also suggest that primary β-oxidation is activated for energy generation. In health, acetyl-CoA from FAO usually enters the TCA cycle and promotes ketogenesis to some extent. However, in human steatosis, the TCA cycle it preferred over ketogenesis.[46] We previously observed that increased glycolytic activity fuels DNL in a mouse model of metabolic-associated fatty liver disease (MAFLD) providing necessary carbon sources.[11] After Cvs, pyruvate derived from glycolysis may be less available, but DNL does not serve as an acetyl-CoA sink. So, acetyl-CoA may be redirected toward the TCA cycle to generate substrates for the ETC, driving hepatic mitochondrial activity. Our findings point directly to mitochondrial function being affected by Cvs and resemble characteristics also observed in MAFLD.

Mitochondrial dynamics are crucial in metabolic adaptation, viability, aging, or bioenergetics,[32] and metabolic diseases prompt mitochondrial function adjustments.[47] Mitochondrial biology responds to stressors cell type-specific with quantitative changes in ATP synthesis, net energy equivalents, and ROS production, as well as qualitative changes in mitochondrial dynamics and substrate preferences.[17] Studies in veterans with PTSD have shown age and stress-related responses in mitochondrial function and copy number in various tissues.[15–17] However, information regarding the liver is rare.[18]

In liver, such as in muscle,[38] the overall mitochondrial content or integrity in quality assessment and key proteins of mitochondrial dynamics involved in fission and fusion[32] were unaltered with no evidence for ROS or increased lipid oxidation immediately following stress. In line, the expression of Nfe2l2, a transcription factor enhancing cellular defense against oxidative stress[48] was decreased immediately after Cvs. Histone-like Tfam and Pgc-1α, control mitochondrial turnover, replication, transcription and FAO pathways.[49,50] In liver, Tfam showed age-dependent but stress-independent gene expression regulation, while Pgc-1α transcription exhibited changes only in the longitudinal analysis of Cvs. This might indicate an ongoing process of lipid metabolic adaptation serving as link to the longitudinal metabolic adaptation.

Changes in hepatic mitochondrial complex protein abundance, respiratory profile, and electron transfer capability were identified in stressed animals. In general, high glycolytic rates in the fed state would bring about higher pyruvate levels, promoting high NADH levels, whereas enhanced mitochondrial FAO inhibits glycolytic rates, but promotes higher acetyl-coA level, which in sum paired with higher NADH levels. Respiratory chain complexes I and II are entry points for electrons derived from substrate breakdown, linking mitochondrial activity to cellular metabolism. Metabolic-derived NADH enters the ETC specifically through CI. Immediately after Cvs, we observed an increase in ATP production efficiency specifically in NADH-fueled CI, supported by a shift in NAD^+/NADH ratio. So, the effects of Cvs on liver substrate turnover, as evidenced by changes in the mitochondrial thermodynamic coupling of CI which may indicate an ongoing adaptation to maximize ATP production. This is further supported by the *η-opt* correlation with activity phase EE and plasma NEFA levels. However, the resulting CI thermodynamic efficiency increases is suggested to maintain cellular phosphorylation potential after Cvs compromises energy conversion efficiency.[51] CI is a reasonble target for Cvs as CI activity was positively correlated with corticosteroid response and liver disease mortality rates,[52] and CI malfunctions were associated with oxidative phosphorylation disorders.[53,54] Similar findings were observed in chronic stress-induced brain metabolic reprogramming and unchanged maximal ATP production despite altered CI activity,[15] as in our model. Notably, in muscle a CII-linked η-opt correlated with EE and plasma NEFA levels, indicating tissue specific metabolic fine-tuning.[38]
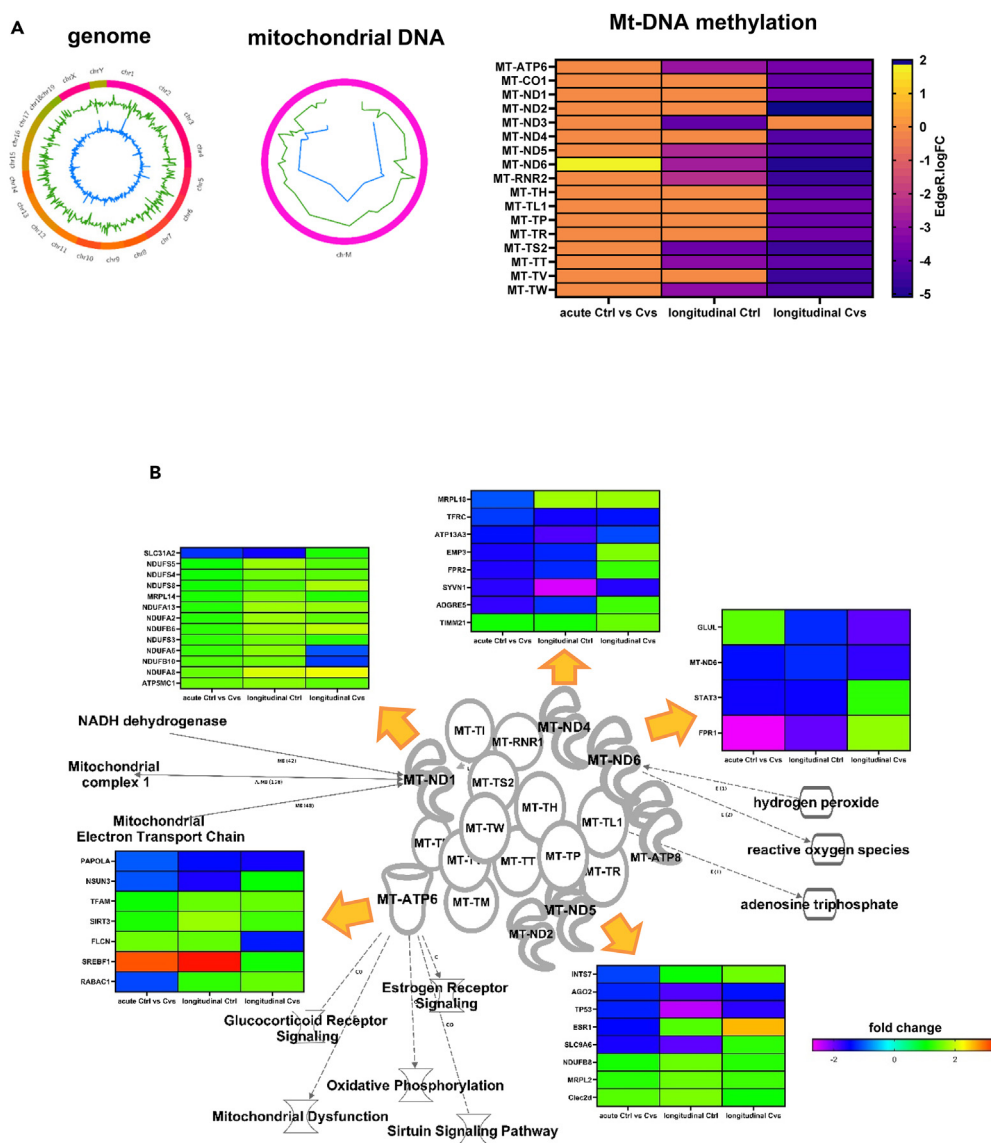
Figure 6. Stress interferes with hepatic mitochondrial gene regulation and function

(A) Circus Plot analyses of longitudinal hepatic methylation differences after acute Cvs and 3-month recovery (longitudinal of either Ctrl or Cvs: acute vs. recovery). Color code: green: longitudinal Cvs, blue: longitudinal Ctrl (Supplement Methylation; n = 3–5/condition). Heatmap of the differential methylation (edgeR.logFC) of all conditions (Table S2; n = 3–5/condition).

(B) Knowledge-based analyses of combined methylation and transcription data centered on the differential methylation of mt-DNA. Heatmaps of transcriptional differences (at least one condition fold change >1.5, p value<0.05 (Table S3)) interfering with main differentially methylated targets in the mitochondria and transcription of knowledge-based interacting molecules.

The enduring metabolic risk following stress-free recovery phases is intriguing. Consistent with human stress studies,[55,56] we previously showed increased hepatic fat and elevated plasma NEFA levels accompanied by increased fatty acid uptake, decreased FAO, and differentially expressed key hepatic steatosis-relegated genes in response to Cvs after the recovery phase.[27]

The immediate mitochondrial response to Cvs aligns with the role of dynamic epigenetic modifications in adapting to environmental changes. The liver predominantly maintains the whole-body one-carbon pools.[21,57] OCM, supplying one-carbon units for nucleotide synthesis and methyl donation in epigenetics, encompasses interconnected pathways in cytosol and mitochondria including the folate cycle, methionine re-methylation, and *trans*-sulfuration. Immediately after Cvs, increased choline module protein abundance suggests glycerophospholipid synthesis[58] for lipid transport, as seen with increased hepatic fatty acid influx.[59] However, folate, *trans*-sulfur, and methionine cycle associated proteins for S-adenosylmethionine (SAM) generation were less abundant immediately after Cvs, suggesting SAM depletion. In line, the overall DNA methylation proportion was lower in the longitudinal observation of mice previously facing Cvs. Changes in the entire methylation

patterns immediately after Cvs were not directly indicative of the observed transcriptional and metabolic alterations compared to unstressed mice. This is expected, as a response to an altered environment relies on immediate effects for transcriptional regulation, such as transcription factor modification or different dimerization processes as also suggested by the expression data. Nevertheless, target genes e.g., of lipid metabolism methylated in metabolic conditions such as hepatic steatosis[60] are differentially expressed in the liver after Cvs.

Although the overall methylation proportion was lower in the longitudinal observation of mice previously exposed to Cvs than in Ctrl, relatively more differences occurred in mtDNA methylation. Unstressed mice also showed overrepresented methylation in certain mtDNA regions during longitudinal comparison but to a lesser degree than Cvs mice.

The most pronounced observation in the variation of methylation levels occurred in the longitudinal analysis of Cvs mice including on mt-DNA. In our analyses, this was accompanied by changes in the respective mitochondrial network transcription patterns. After Cvs, mt-Nd6 transcription followed the methylation pattern, suggesting its involvement in Cvs-induced cellular adaptation. So, the differences in mtDNA methylation levels are accompanied by differential transcriptional patterns and support the observation that finally the energetic reserve of hepatocytes is lost after the recovery phase only after a previous Cvs experience. This observation is further supported by the energy phenotype analyses, where hepatocytes at basal state show no difference in the activity of glycolytic and oxidative pathways (ECAR vs. OCR), independent of acute Cvs or recovery group. In contrast, uncoupling of the cells, to create a state of low mitochondrial membrane potential, showed that hepatocytes derived from recovery group livers are no longer able to switch their energy source to oxidative pathways when compared to acute Cvs livers.

The impact of mtDNA methylation is still discussed. Reports indicate that mtDNA methylation massively fights technical issues, does not exist, or that ^{met}C levels are very low in mtDMA.[61–64] However, of all studies discussing the presence of mt-DNA methylation the consent may be, that methylation levels are low and technical bias according to the methods used may be high.

Although mtDNA methylation is clearly debated, also experimental evidence links it to age, health, and environmental responses.[22,60,65–67] Harsh environmental factors such as intoxication induce the hypomethylation of mt-TF, mt-RMR1, mt-ND6, and the regulatory D loop regulating mitochondrial transcription and DNA replication.[68] We observed unaltered methylation in the regulatory D loop region after Cvs matches the observed mtDNA copy number stability in the study and previous findings.[69,70]

MtDNA methylation potentially impacts mitochondrial gene expression, and was associated with metabolic diseases such as diabetic retinopathy, cardiovascular disease, and hepatic steatosis.[60] However, there is evidence suggesting that changes in the epigenetic landscape contribute to mitochondrial dysfunction.[71] Altered methylation near the mt-Nd6 gene has previously been observed in diabetes or hepatic steatosis where expression negatively correlated to severity.[67,72,73] Similar to our findings, this hypermethylation was associated with the altered transcription of the corresponding gene in liver biopsies of patients with NASH, emphasizing the regulatory importance of MT-ND6, a subunit of complex I of the mitochondrial respiratory chain.[73] In our study, mt-Nd6 showed moderate methylation in aging in controls, but aggravated methylation after Cvs recovery, as such mimicking processes observed in hepatic steatosis progression.

In summary, our findings indicate that immediately after Cvs liver mitochondrial oxidative phosphorylation is affected by increased thermodynamic efficiency of CI. This effect is associated with reduced EE and elevated NEFAs, particularly cC18:2 levels. While the stress period alone marginally affects methylation patterns, the metabolic changes manifest in methylome adaptation in the stressed cohort. This involves decreased overall methylation, altered mtDNA methylation, and related mitochondrial transcriptional networks. The energy map illustrates a loss of metabolic flexibility in liver as a sustainable consequence of former chronic stress exposure even after stress recovery. Our study indicates that methylation is a consequence of immediate Cvs-induced hepatic energy metabolism fine-tuning, retaining environmental information for adaptation to altered life conditions, rather than a primary driving force to modulate the stress adaptation. So, even short periods of chronic stress also affect molecular mechanisms associated with the progression of metabolic diseases such as diabetes or NAFLD and join the list of factors leading to the loss of epigenetic information as a postulated key mechanism in disease and aging.

Limitations of the study

Technical issue may rely on relative changes and on mitochondrial enrichment in the protein fractions during the general procedure of label-free proteomic analyses and the mitochondrial functionality assays. These were circumvented by defined protein amount input and the use of the accepted marker of mitochondrial content CS for normalization and pathway rather than single molecule analyses. Methylome analyses were performed in sheered, immunprecipitated ^{met}C containing DNA fragments, circumventing technical issues on bisulfite-mediated procedures especially in regard to mtDNA. Other techniques as nanopore sequencing may also help to overcome bisulfite-based bias on mtDNA methylation analyses. Our study must speculate on how post-Cvs hypomethylation influences mtDNA transcription or stability and whether it is an active mt-methyltransferases-driven process or a result of diminished mitochondrial renewal, necessitating further research, favourable in humans. The focus of the analyses on the promoter areas should in principle enable the transfer to the human system. We use a standardized pre-clinical model to analyze chronic stress. Nevertheless, this allows us to study the effects of cellular adaptations on maintaining energy balance, minimizing confounding factors present in more complex clinical studies.

STAR★METHODS

Detailed methods are provided in the online version of this paper and include the following:

- KEY RESOURCES TABLE
- RESOURCE AVAILABILITY

SUPPLEMENTAL INFORMATION

Supplemental information can be found online at https://doi.org/10.1016/j.isci.2024.109276.

AUTHOR CONTRIBUTIONS

Aleksandra Nikolic, Pia Fahlbusch, Jörg Kotzka, and Birgit Knebel performed conceptualization and design of the study. Aleksandra Nikolic, Natalie Wahlers, Nele-Kathrien Riffelmann, Matthias Dille, Pia Fahlbusch and Sylvia Jacob researched physiological, transcriptome and methylation data. Ulrike Kettel and Sonja Hartwig researched proteomic data. Martina Schiller researched lipidomic data. Jörg Kotzka and Birgit Knebel performed bioinformatics data analyses. The first draft of the article was written by Aleksandra Nikolic, Pia Fahlbusch, Jörg Kotzka and Birgit Knebel. All authors commented on previous versions of the article. Hadi Al-Hasani, Jörg Kotzka, and Birgit Knebel supervised the study. Aleksandra Nikolic/Pia Fahlbusch and Jörg Kotzka/Birgit Knebel contributed equally to this work. All authors have read and approved the final article.

DECLARATION OF INTERESTS

The authors declare no competing interest.

REFERENCES

1. Goldbacher, E.M., Bromberger, J., and Matthews, K.A. (2009). Lifetime history of major depression predicts the development of the metabolic syndrome in middle-aged women. Psychosom. Med. *71*, 266–272. https://doi.org/10.1097/PSY.0b013e318197a4d5.

2. Heppner, P.S., Crawford, E.F., Haji, U.A., Afari, N., Hauger, R.L., Dashevsky, B.A., Horn, P.S., Nunnink, S.E., and Baker, D.G. (2009). The association of posttraumatic stress disorder and metabolic syndrome: a study of increased health risk in veterans. BMC Med. *7*, 1. https://doi.org/10.1186/1741-7015-7-1.

3. Lindqvist, D., Dhabhar, F.S., Mellon, S.H., Yehuda, R., Grenon, S.M., Flory, J.D., Bierer, L.M., Abu-Amara, D., Coy, M., Makotkine, I., et al. (2017). Increased pro-inflammatory milieu in combat related PTSD - A new cohort replication study. Brain Behav. Immun. *59*, 260–264. https://doi.org/10.1016/j.bbi.2016.09.012.

4. Mellon, S.H., Bersani, F.S., Lindqvist, D., Hammamieh, R., Donohue, D., Dean, K., Jett, M., Yehuda, R., Flory, J., Reus, V.I., et al. (2019). Metabolomic analysis of male combat veterans with post traumatic stress disorder. PLoS One *14*, e0213839. https://doi.org/10.1371/journal.pone.0213839.

5. Mellon, S.H., Gautam, A., Hammamieh, R., Jett, M., and Wolkowitz, O.M. (2018). Metabolism, Metabolomics, and Inflammation in Posttraumatic Stress Disorder. Biol. Psychiatr. *83*, 866–875. https://doi.org/10.1016/j.biopsych.2018.02.007.

6. Lacal, I., and Ventura, R. (2018). Epigenetic Inheritance: Concepts, Mechanisms and Perspectives. Front. Mol. Neurosci. *11*, 292. https://doi.org/10.3389/fnmol.2018.00292.

7. Fall, C.H.D., and Kumaran, K. (2019). Metabolic programming in early life in humans. Philos. Trans. R. Soc. Lond. B Biol. Sci. *374*, 20180123. https://doi.org/10.1098/rstb.2018.0123.

8. Grilo, L.F., Tocantins, C., Diniz, M.S., Gomes, R.M., Oliveira, P.J., Matafome, P., and Pereira, S.P. (2021). Metabolic Disease Programming: From Mitochondria to Epigenetics, Glucocorticoid Signalling and Beyond. Eur. J. Clin. Invest. *51*, e13625. https://doi.org/10.1111/eci.13625.

9. Heijmans, B.T., Tobi, E.W., Stein, A.D., Putter, H., Blauw, G.J., Susser, E.S., Slagboom, P.E., and Lumey, L.H. (2008). Persistent epigenetic differences associated with prenatal exposure to famine in humans. Proc. Natl. Acad. Sci. USA *105*, 17046–17049. https://doi.org/10.1073/pnas.0806560105.

10. Cheng, Z., Zheng, L., and Almeida, F.A. (2018). Epigenetic reprogramming in metabolic disorders: nutritional factors and beyond. J. Nutr. Biochem. *54*, 1–10. https://doi.org/10.1016/j.jnutbio.2017.10.004.

11. Fahlbusch, P., Nikolic, A., Hartwig, S., Jacob, S., Kettel, U., Köllmer, C., Al-Hasani, H., Lehr, S., Müller-Wieland, D., Knebel, B., and Kotzka, J. (2022). Adaptation of Oxidative Phosphorylation Machinery Compensates for Hepatic Lipotoxicity in Early Stages of MAFLD. Int. J. Mol. Sci. *23*, 6873. https://doi.org/10.3390/ijms23126873.

12. Ling, C., and Rönn, T. (2019). Epigenetics in Human Obesity and Type 2 Diabetes. Cell Metabol. *29*, 1028–1044. https://doi.org/10.1016/j.cmet.2019.03.009.

13. Ouni, M., and Schürmann, A. (2020). Epigenetic contribution to obesity. Mamm. Genome *31*, 134–145. https://doi.org/10.1007/s00335-020-09835-3.

14. Rogers, J.M. (2019). Smoking and pregnancy: Epigenetics and developmental origins of the metabolic syndrome. Birth Defects Res. *111*, 1259–1269. https://doi.org/10.1002/bdr2.1550.

15. Emmerzaal, T.L., Preston, G., Geenen, B., Verweij, V., Wiesmann, M., Vasileiou, E., Grüter, F., de Groot, C., Schoorl, J., de Veer, R., et al. (2020). Impaired mitochondrial complex I function as a candidate driver in the biological stress response and a concomitant stress-induced brain metabolic reprogramming in male mice. Transl. Psychiatry *10*, 176. https://doi.org/10.1038/s41398-020-0858-y.

16. Picard, M., and McEwen, B.S. (2018). Psychological Stress and Mitochondria: A Conceptual Framework. Psychosom. Med. *80*, 126–140. https://doi.org/10.1097/psy.0000000000000544.

17. Picard, M., and McEwen, B.S. (2018). Psychological Stress and Mitochondria: A Systematic Review. Psychosom. Med. *80*, 141–153. https://doi.org/10.1097/PSY.0000000000000545.

18. Rabasa, C., Askevik, K., Schéle, E., Hu, M., Vogel, H., and Dickson, S.L. (2019). Divergent Metabolic Effects of Acute Versus Chronic Repeated Forced Swim Stress in the Rat. Obesity *27*, 427–433. https://doi.org/10.1002/oby.22390.

19. Rolfe, D.F., and Brown, G.C. (1997). Cellular energy utilization and molecular origin of standard metabolic rate in mammals. Physiol. Rev. *77*, 731–758. https://doi.org/10.1152/physrev.1997.77.3.731.

20. Bohovych, I., and Khalimonchuk, O. (2016). Sending Out an SOS: Mitochondria as a Signaling Hub. Front. Cell Dev. Biol. *4*, 109. https://doi.org/10.3389/fcell.2016.00109.

21. Ducker, G.S., and Rabinowitz, J.D. (2017). One-Carbon Metabolism in Health and Disease. Cell Metabol. *25*, 27–42. https://doi.org/10.1016/j.cmet.2016.08.009.

22. Sharma, J., Kumari, R., Bhargava, A., Tiwari, R., and Mishra, P.K. (2021). Mitochondrial-induced Epigenetic Modifications: From Biology to Clinical Translation. Curr. Pharmaceut. Des. *27*, 159–176. https://doi.org/10.2174/1381612826666200826165735.

23. Lewis, M.T., Kasper, J.D., Bazil, J.N., Frisbee, J.C., and Wiseman, R.W. (2019). Quantification of Mitochondrial Oxidative Phosphorylation in Metabolic Disease: Application to Type 2 Diabetes. Int. J. Mol. Sci. *20*, 5271. https://doi.org/10.3390/ijms20215271.

24. Rovira-Llopis, S., Bañuls, C., Diaz-Morales, N., Hernandez-Mijares, A., Rocha, M., and Victor, V.M. (2017). Mitochondrial dynamics in type 2 diabetes: Pathophysiological implications. Redox Biol. *11*, 637–645. https://doi.org/10.1016/j.redox.2017.01.013.

25. Vezza, T., Díaz-Pozo, P., Canet, F., de Marañón, A.M., Abad-Jiménez, Z., García-Gargallo, C., Roldan, I., Solá, E., Bañuls, C., López-Domènech, S., et al. (2022). The Role of Mitochondrial Dynamic Dysfunction in Age-Associated Type 2 Diabetes. World J. Mens Health *40*, 399–411. https://doi.org/10.5534/wjmh.210146.

26. Jelenik, T., Dille, M., Müller-Lühlhoff, S., Kabra, D.G., Zhou, Z., Binsch, C., Hartwig, S., Lehr, S., Chadt, A., Peters, E.M.J., et al. (2018). FGF21 regulates insulin sensitivity following long-term chronic stress. Mol. Metabol. *16*, 126–138. https://doi.org/10.1016/j.molmet.2018.06.012.

27. Dille, M., Nikolic, A., Wahlers, N., Fahlbusch, P., Jacob, S., Hartwig, S., Lehr, S., Kabra, D., Klymenko, O., Al-Hasani, H., et al. (2022). Long-term adjustment of hepatic lipid metabolism after chronic stress and the role of FGF21. Biochim. Biophys. Acta, Mol. Basis Dis. *1868*, 166286. https://doi.org/10.1016/j.bbadis.2021.166286.

28. McLaughlin, K.L., Hagen, J.T., Coalson, H.S., Nelson, M.A.M., Kew, K.A., Wooten, A.R., and Fisher-Wellman, K.H. (2020). Novel approach to quantify mitochondrial content and intrinsic bioenergetic efficiency across organs. Sci. Rep. *10*, 17599. https://doi.org/10.1038/s41598-020-74718-1.

29. Kuznetsov, A.V., Strobl, D., Ruttmann, E., Königsrainer, A., Margreiter, R., and Gnaiger, E. (2002). Evaluation of mitochondrial respiratory function in small biopsies of liver. Anal. Biochem. *305*, 186–194. https://doi.org/10.1006/abio.2002.5658.

30. Larsen, S., Nielsen, J., Hansen, C.N., Nielsen, L.B., Wibrand, F., Stride, N., Schroder, H.D., Boushel, R., Helge, J.W., Dela, F., and Hey-Mogensen, M. (2012). Biomarkers of mitochondrial content in skeletal muscle of healthy young human subjects. J. Physiol. *590*, 3349–3360. https://doi.org/10.1113/jphysiol.2012.230185.

31. Reichmann, H., Hoppeler, H., Mathieu-Costello, O., von Bergen, F., and Pette, D. (1985). Biochemical and ultrastructural changes of skeletal muscle mitochondria after chronic electrical stimulation in rabbits. Pflügers Archiv *404*, 1–9. https://doi.org/10.1007/BF00581484.

32. Roca-Portoles, A., and Tait, S.W.G. (2021). Mitochondrial quality control: from molecule to organelle. Cell. Mol. Life Sci. *78*, 3853–3866. https://doi.org/10.1007/s00018-021-03775-0.

33. Péronnet, F., and Massicotte, D. (1991). Table of nonprotein respiratory quotient: an update. Can. J. Sport Sci. *16*, 23–29.

34. Beaupere, C., Liboz, A., Fève, B., Blondeau, B., and Guillemain, G. (2021). Molecular Mechanisms of Glucocorticoid-Induced Insulin Resistance. Int. J. Mol. Sci. *22*, 623. https://doi.org/10.3390/ijms22020623.

35. van Bodegom, M., Homberg, J.R., and Henckens, M.J.A.G. (2017). Modulation of the Hypothalamic-Pituitary-Adrenal Axis by Early Life Stress Exposure. Front. Cell. Neurosci. *11*, 87. https://doi.org/10.3389/fncel.2017.00087.

36. van den Berk-Clark, C., Secrest, S., Walls, J., Hallberg, E., Lustman, P.J., Schneider, F.D., and Scherrer, J.F. (2018). Association between posttraumatic stress disorder and lack of exercise, poor diet, obesity, and co-occuring smoking: A systematic review and meta-analysis. Health Psychol. *37*, 407–416. https://doi.org/10.1037/hea0000593.

37. Yaribeygi, H., Maleki, M., Butler, A.E., Jamialahmadi, T., and Sahebkar, A. (2022). Molecular mechanisms linking stress and insulin resistance. EXCLI J *21*, 317–334. https://doi.org/10.17179/excli2021-4382.

38. Nikolic, A., Fahlbusch, P., Wahlers, N., Riffelmann, N.K., Jacob, S., Hartwig, S., Kettel, U., Dille, M., Al-Hasani, H., Kotzka, J., and Knebel, B. (2023). Chronic stress targets mitochondrial respiratory efficiency in the skeletal muscle of C57BL/6 mice. Cell. Mol. Life Sci. *80*, 108. https://doi.org/10.1007/s00018-023-04761-4.

39. Kuti, D., Winkler, Z., Horváth, K., Juhász, B., Szilvásy-Szabó, A., Fekete, C., Ferenczi, S., and Kovács, K.J. (2022). The metabolic stress response: Adaptation to acute-repeated- and chronic challenges in mice. iScience *25*, 104693. https://doi.org/10.1016/j.isci.2022.104693.

40. Brown, Z.J., Fu, Q., Ma, C., Kruhlak, M., Zhang, H., Luo, J., Heinrich, B., Yu, S.J., Zhang, Q., Wilson, A., et al. (2018). Carnitine palmitoyltransferase gene upregulation by linoleic acid induces CD4(+) T cell apoptosis promoting HCC development. Cell Death Dis. *9*, 620. https://doi.org/10.1038/s41419-018-0687-6.

41. Crane, H., Gofton, C., Sharma, A., and George, J. (2023). MAFLD: an optimal framework for understanding liver cancer phenotypes. J. Gastroenterol. *58*, 947–964. https://doi.org/10.1007/s00535-023-02021-7.

42. Chuang, J.C., Cui, H., Mason, B.L., Mahgoub, M., Bookout, A.L., Yu, H.G., Perello, M., Elmquist, J.K., Repa, J.J., Zigman, J.M., and Lutter, M. (2010). Chronic social defeat stress disrupts regulation of lipid synthesis. J. Lipid Res. *51*, 1344–1353. https://doi.org/10.1194/jlr.M002196.

43. Lindqvist, D., Dhabhar, F.S., James, S.J., Hough, C.M., Jain, F.A., Bersani, F.S., Reus, V.I., Verhoeven, J.E., Epel, E.S., Mahan, L., et al. (2017). Oxidative stress, inflammation and treatment response in major depression. Psychoneuroendocrinology *76*, 197–205. https://doi.org/10.1016/j.psyneuen.2016.11.031.

44. Hue, L., and Taegtmeyer, H. (2009). The Randle cycle revisited: a new head for an old hat. Am. J. Physiol. Endocrinol. Metab. *297*, E578–E591. https://doi.org/10.1152/ajpendo.00093.2009.

45. Mazziotti, G., Gazzaruso, C., and Giustina, A. (2011). Diabetes in Cushing syndrome: basic and clinical aspects. Trends Endocrinol. Metabol. *22*, 499–506. https://doi.org/10.1016/j.tem.2011.09.001.

46. Fletcher, J.A., Deja, S., Satapati, S., Fu, X., Burgess, S.C., and Browning, J.D. (2019). Impaired ketogenesis and increased acetyl-CoA oxidation promote hyperglycemia in human fatty liver. JCI Insight *5*, e127737. https://doi.org/10.1172/jci.insight.127737.

47. Wang, D., Ji, D.C., Yu, C.Y., Wu, D.N., and Qi, L. (2023). Research progress on the mitochondrial mechanism of age-related non-alcoholic fatty liver. World J. Gastroenterol. *29*, 1982–1993. https://doi.org/10.3748/wjg.v29.i13.1982.

48. Vomhof-Dekrey, E.E., and Picklo, M.J., Sr. (2012). The Nrf2-antioxidant response element pathway: a target for regulating energy metabolism. J. Nutr. Biochem. *23*,

1201–1206. https://doi.org/10.1016/j.jnutbio.2012.03.005.

49. Chew, K., and Zhao, L. (2021). Interactions of Mitochondrial Transcription Factor A with DNA Damage: Mechanistic Insights and Functional Implications. Genes *12*, 1246. https://doi.org/10.3390/genes12081246.

50. Morris, E.M., Meers, G.M.E., Booth, F.W., Fritsche, K.L., Hardin, C.D., Thyfault, J.P., and Ibdah, J.A. (2012). PGC-1alpha overexpression results in increased hepatic fatty acid oxidation with reduced triacylglycerol accumulation and secretion. Am. J. Physiol. Gastrointest. Liver Physiol. *303*, G979–G992. https://doi.org/10.1152/ajpgi.00169.2012.

51. Stucki, J.W. (1980). The optimal efficiency and the economic degrees of coupling of oxidative phosphorylation. Eur. J. Biochem. *109*, 269–283. https://doi.org/10.1111/j.1432-1033.1980.tb04792.x.

52. Solis-Munoz, P., de la Flor-Robledo, M., Garcia-Ruiz, I., Fernandez-Garcia, C.E., Gonzalez-Rodriguez, A., Shah, N., Bataller, R., Heneghan, M., Garcia-Monzon, C., and Solis-Herruzo, J.A. (2023). Mitochondrial respiratory chain activity is associated with severity, corticosteroid response and prognosis of alcoholic hepatitis. Aliment. Pharmacol. Ther. *57*, 1131–1142. https://doi.org/10.1111/apt.17434.

53. Antonicka, H., Ogilvie, I., Taivassalo, T., Anitori, R.P., Haller, R.G., Vissing, J., Kennaway, N.G., and Shoubridge, E.A. (2003). Identification and characterization of a common set of complex I assembly intermediates in mitochondria from patients with complex I deficiency. J. Biol. Chem. *278*, 43081–43088. https://doi.org/10.1074/jbc.M304998200.

54. Loeffen, J.L., Smeitink, J.A., Trijbels, J.M., Janssen, A.J., Triepels, R.H., Sengers, R.C., and van den Heuvel, L.P. (2000). Isolated complex I deficiency in children: clinical, biochemical and genetic aspects. Hum. Mutat. *15*, 123–134. https://doi.org/10.1002/(SICI)1098-1004(200002)15:2<123::AID-HUMU1>3.0.CO;2-P.

55. Kang, D., Zhao, D., Ryu, S., Guallar, E., Cho, J., Lazo, M., Shin, H., Chang, Y., and Sung, E. (2020). Perceived stress and non-alcoholic fatty liver disease in apparently healthy men and women. Sci. Rep. *10*, 38. https://doi.org/10.1038/s41598-019-57036-z.

56. Pagoto, S.L., Schneider, K.L., Bodenlos, J.S., Appelhans, B.M., Whited, M.C., Ma, Y., and Lemon, S.C. (2012). Association of post-traumatic stress disorder and obesity in a nationally representative sample. Obesity *20*, 200–205. https://doi.org/10.1038/oby.2011.318.

57. Clare, C.E., Brassington, A.H., Kwong, W.Y., and Sinclair, K.D. (2019). One-Carbon Metabolism: Linking Nutritional Biochemistry to Epigenetic Programming of Long-Term Development. Annu. Rev. Anim. Biosci. *7*, 263–287. https://doi.org/10.1146/annurev-animal-020518-115206.

58. Wright, M.M., Howe, A.G., and Zaremberg, V. (2004). Cell membranes and apoptosis: role of cardiolipin, phosphatidylcholine, and anticancer lipid analogues. Biochem. Cell.

Biol. *82*, 18–26. https://doi.org/10.1139/o03-092.

59. Shahsavari, A., D'Occhio, M.J., and Al Jassim, R. (2016). The role of rumen-protected choline in hepatic function and performance of transition dairy cows. Br. J. Nutr. *116*, 35–44. https://doi.org/10.1017/S0007114516001641.

60. Zhang, N., Tian, X., Yan, T., Wang, H., Zhang, D., Lin, C., Liu, Q., and Jiang, S. (2023). Insights into the role of nucleotide methylation in metabolic-associated fatty liver disease. Front. Immunol. *14*, 1148722. https://doi.org/10.3389/fimmu.2023.1148722.

61. Guitton, R., Nido, G.S., and Tzoulis, C. (2022). No evidence of extensive non-CpG methylation in mtDNA. Nucleic Acids Res. *50*, 9190–9194. https://doi.org/10.1093/nar/gkac701.

62. Matsuda, S., Yasukawa, T., Sakaguchi, Y., Ichiyanagi, K., Unoki, M., Gotoh, K., Fukuda, K., Sasaki, H., Suzuki, T., and Kang, D. (2018). Accurate estimation of 5-methylcytosine in mammalian mitochondrial DNA. Sci. Rep. *8*, 5801. https://doi.org/10.1038/s41598-018-24251-z.

63. Owa, C., Poulin, M., Yan, L., and Shioda, T. (2018). Technical adequacy of bisulfite sequencing and pyrosequencing for detection of mitochondrial DNA methylation: Sources and avoidance of false-positive detection. PLoS One *13*, e0192722. https://doi.org/10.1371/journal.pone.0192722.

64. Shao, Z., Han, Y., and Zhou, D. (2023). Optimized bisulfite sequencing analysis reveals the lack of 5-methylcytosine in mammalian mitochondrial DNA. BMC Genom. *24*, 439. https://doi.org/10.1186/s12864-023-09541-9.

65. Liu, Y.F., Zhu, J.J., Yu Tian, X., Liu, H., Zhang, T., Zhang, Y.P., Xie, S.A., Zheng, M., Kong, W., Yao, W.J., et al. (2020). Hypermethylation of mitochondrial DNA in vascular smooth muscle cells impairs cell contractility. Cell Death Dis. *11*, 35. https://doi.org/10.1038/s41419-020-2240-7.

66. Sharma, N., Pasala, M.S., and Prakash, A. (2019). Mitochondrial DNA: Epigenetics and environment. Environ. Mol. Mutagen. *60*, 668–682. https://doi.org/10.1002/em.22319.

67. Mposhi, A., Cortés-Mancera, F., Heegsma, J., de Meijer, V.E., van de Sluis, B., Sydor, S., Bechmann, L.P., Theys, C., de Rijk, P., De Pooter, T., et al. (2023). Mitochondrial DNA methylation in metabolic associated fatty liver disease. Front. Nutr. *10*, 964337. https://doi.org/10.3389/fnut.2023.964337.

68. Sanyal, T., Bhattacharjee, P., Bhattacharjee, S., and Bhattacharjee, P. (2018). Hypomethylation of mitochondrial D-loop and ND6 with increased mitochondrial DNA copy number in the arsenic-exposed population. Toxicology *408*, 54–61. https://doi.org/10.1016/j.tox.2018.06.012.

69. Gao, J., Wen, S., Zhou, H., and Feng, S. (2015). De-methylation of displacement loop of mitochondrial DNA is associated with increased mitochondrial copy number and nicotinamide adenine dinucleotide subunit 2 expression in colorectal cancer. Mol. Med. Rep. *12*, 7033–7038. https://doi.org/10.3892/mmr.2015.4256.

70. Stoccoro, A., Mosca, L., Carnicelli, V., Cavallari, U., Lunetta, C., Marocchi, A., Migliore, L., and Coppedè, F. (2018). Mitochondrial DNA copy number and D-loop region methylation in carriers of amyotrophic lateral sclerosis gene mutations. Epigenomics *10*, 1431–1443. https://doi.org/10.2217/epi-2018-0072.

71. Guha, S., Sesili, S., Mir, I.H., and Thirunavukkarasu, C. (2023). Epigenetics and mitochondrial dysfunction insights into the impact of the progression of non-alcoholic fatty liver disease. Cell Biochem. Funct. *41*, 4–19. https://doi.org/10.1002/cbf.3763.

72. Lapp, H.E., Bartlett, A.A., and Hunter, R.G. (2019). Stress and glucocorticoid receptor regulation of mitochondrial gene expression. J. Mol. Endocrinol. *62*, R121–R128. https://doi.org/10.1530/JME-18-0152.

73. Pirola, C.J., Gianotti, T.F., Burgueño, A.L., Rey-Funes, M., Loidl, C.F., Mallardi, P., Martino, J.S., Castaño, G.O., and Sookoian, S. (2013). Epigenetic modification of liver mitochondrial DNA is associated with histological severity of nonalcoholic fatty liver disease. Gut *62*, 1356–1363. https://doi.org/10.1136/gutjnl-2012-302962.

74. Malik, A.N., Czajka, A., and Cunningham, P. (2016). Accurate quantification of mouse mitochondrial DNA without co-amplification of nuclear mitochondrial insertion sequences. Mitochondrion *29*, 59–64. https://doi.org/10.1016/j.mito.2016.05.003.

75. Lienhard, M., Grimm, C., Morkel, M., Herwig, R., and Chavez, L. (2014). MEDIPS: genome-wide differential coverage analysis of sequencing data derived from DNA enrichment experiments. Bioinformatics *30*, 284–286.

76. Akie, T.E., and Cooper, M.P. (2015). Determination of Fatty Acid Oxidation and Lipogenesis in Mouse Primary Hepatocytes. J. Vis. Exp. e52982. https://doi.org/10.3791/52982.

77. Lehr, S., Kotzka, J., Avci, H., Knebel, B., Muller, S., Hanisch, F.G., Jacob, S., Haak, C., Susanto, F., and Muller-Wieland, D. (2005). Effect of sterol regulatory element binding protein-1a on the mitochondrial protein pattern in human liver cells detected by 2D-DIGE. Biochemistry *44*, 5117–5128. https://doi.org/10.1021/bi0479656.

78. Quiros, P.M., Goyal, A., Jha, P., and Auwerx, J. (2017). Analysis of mtDNA/nDNA Ratio in Mice. Curr. Protoc. Mol. Biol. *7*, 47–54. https://doi.org/10.1002/cpmo.21.

79. Krämer, A., Green, J., Pollard, J., Jr., and Tugendreich, S. (2014). Causal analysis approaches in Ingenuity Pathway Analysis. Bioinformatics *30*, 523–530. https://doi.org/10.1093/bioinformatics/btt703.

80. Mi, H., Muruganujan, A., Huang, X., Ebert, D., Mills, C., Guo, X., and Thomas, P.D. (2019). Protocol Update for large-scale genome and gene function analysis with the PANTHER classification system (v.14.0). Nat. Protoc. *14*, 703–721. https://doi.org/10.1038/s41596-019-0128-8.

81. Rasche, H., and Hiltemann, S. (2020). Galactic Circos: User-friendly Circos plots within the Galaxy platform. GigaScience *9*, giaa065. https://doi.org/10.1093/gigascience/giaa065.

STAR★METHODS

KEY RESOURCES TABLE

REAGENT or RESOURCE	SOURCE	IDENTIFIER
Chemicals, peptides, and recombinant proteins		
^{14}C-acetate, Acetic Acid, Sodium Salt [1-^{14}C]	Perkin Elmer	Cat#NEC084H001MC; CAS: 993-04-4
^{14}C-palmitate, Palmitic Acid, [1-^{14}C]	Perkin Elmer	Cat#NEC075H250UC
(+)-Etomoxir, sodium salt hydrate, ≥98% (HPLC), powder	Merck KGaA	Cat#E1905; CAS: 828934-41-4
Antimycin A from Streptomyces sp.	Merck KGaA	Cat#A8674; CAS: 1397-94-0
Adenosine 5′-diphosphate monopotassium salt dehydrate	Merck KGaA	Cat#A5285; CAS: 72696-48-1
Carbonyl cyanide 4-(trifluoromethoxy)phenylhydrazone (FCCP, ≥98% (TLC), powder)	Merck KGaA	Cat#C2920; CAS: 370-86-5
Succinic acid	Merck KGaA	Cat#S3674; CAS: 110-15-6
Pyruvic acid	Merck KGaA	Cat#107360; CAS: 127-17-3
L-(−)-Malic acid	Merck KGaA	Cat#02288; CAS: 97-67-6
N,N,N′,N′-Tetramethyl-1,4-phenylenediamine (TMPD)	Merck KGaA	Cat#8211010005
Ascorbic acid	Merck KGaA	Cat#A1300000; CAS: 50-81-7
Oligomycin A, ≥95% (HPLC)	Merck KGaA	Cat#75351; CAS: 579-13-5
Rotenone, ≥95%	Merck KGaA	Cat#R8875; CAS: 83-79-4
Critical commercial assays		
Bio-Plex Pro™, mouse Diabetes 8-plex	Bio-Rad	Cat#171F7001M
Lactate Assay Kit	Sigma-Aldrich	Cat#MAK064
Glucose Assay Kit	Sigma-Aldrich	Cat#MAK263
Glutamate Assay Kit	Sigma-Aldrich	Cat#MAK330
Triglyceride Quantification Kit	Sigma-Aldrich	Cat#MAK044
ß-hydroxybutyrate Assay Kit	Sigma-Aldrich	Cat#MAK041
OxiSelect™ TBARS Assay (MDA Quantification)	Cell Biolabs	Cat#STA-330
Cytochrom-C-Oxidase-Assay-Kit	Sigma-Aldrich	Cat#CYTOCOX1
Citrate synthase (CS) activity Kit	Merck KGaA	Cat#CS0720
NAD/NADH-GloTM Assay,	Promega	Cat#G9071
MTase-Glo Methyltransferase assay,	Promega	Cat#V7601
FAD+ (FAD Assay Kit)	Abcam	Cat#Ab204710
SIRT-Glo Assay System, Promega, Germany	Promega	Cat#G4650
Mouse Gene (MTA) arrays	Thermo Fisher Scientific	Cat#902512
EpiXploreTM Methylated DNA Enrichment Kit	Takara Bio Europe	Cat#631962
NEB Ultra-II Library kit	NewEngland BioLabs	Cat#E7645L
Randox Triglycerides	RANDOX Laboratories	Cat#TR210
Seahorse XFe24 FluxPak	Agilent Technologie	Cat#102340-100
Seahorse XFe96 FluxPak	Agilent Technologies	Cat#102416-100
GOTaq®QPCR SybrGreen	Promega	Cat#A6001

Continued

REAGENT or RESOURCE	SOURCE	IDENTIFIER
Deposited data		
Proteome data	PRIDE partner repository https://www.proteomexchange.org/	PXD042472
Transcriptiome data	https://www.ncbi.nlm.nih.gov/geo/query/acc.cgi?acc= assession number	GSE23494 transcriptome data or GSE235424 for the superseries.
Methylome data	https://www.ncbi.nlm.nih.gov/geo/query/acc.cgi?acc= assession number	GSE235423 for methylation data and GSE235424 for the superseries
Experimental models: Organisms/strains		
Mouse: C57BL/6	The Jackson Laboratory	RRID:MGI:7264769
Oligonucleotides		
MT-ND 1 double dye probe CCAATACGCCCTTTAACAACCTC	FP-5'-CTACAACCATTTGCAGACGC	RP-5'-GGAACTCATAGACTTAATGC T
LPL double dye probe CTTTGAGTATGCAGAAGCCC	FP-5'-GGTTTGGATCCAGCTGGGCC	RP-5'-GATTCCAATACTTCGACCAGG
mMito Malik et al.[74]	5' CTA-GAA-ACC-CCG-AAA-CCA-AA 3'	5' CCA-GCT-ATC-ACC-AAG-CTC-GT 3'
mB2M (ß-microglobulin) Malik et al.[74]	5' ATG-GGA-AGC-CGA-ACA-TAC-TG 3'	5' CAG-TCT-CAG-TGG-GGG-TGA-AT 3'
Software and algorithms		
Proteome Discoverer, Version 2.5	Thermo Fisher Scientific	https://www.thermofisher.com
Spectronaut™ Pulsar, Version 17	Biognosys	https://biognosys.com/software/spectronaut/
Transcriptome Analysis Console™ , Version 4.01	Thermo Fisher Scientific	https://www.thermofisher.com/de/de/home/life-science/microarray-analysis
Illumina Dragen®, Version 3.9.5	Illumina	https://support.illumina.com/downloads/dragen-workflow-fastq-installer.html
DRAGEN Germline pipeline, Version 3.2.8	Illumina	https://support.illumina.com/downloads/dragen-workflow-fastq-installer.html
DRAGEN Reference builder, Version 3.10.4	Illumina	https://support.illumina.com/downloads/dragen-workflow-fastq-installer.html
Fast Q toolkit pipeline, Version 1.0.0	Illumina	https://support.illumina.com/downloads/dragen-workflow-fastq-installer.html
R/Bioconductor package ChIPseeker, Version 1.18.0	Bioconductor	http://galaxyproject.org
R package MeDIP	Lienhard M et al.[75]	R/Bioconductor package
R packages Circus plot, Version 0.69	Galaxy.org platform	http://galaxyproject.org
IPA® (QIAGEN Inc.,), Spring release 2023	IPA	https://digitalinsights.qiagen.com/IPA
Panther™, Version 17	PANTHER	http://www.pantherdb.org/
GraphPad Prism, Version 9.5.0	Dotmatics	https://www.graphpad.com/d.com
Tecan i-control, Version 1.6.19.0	Tecan Group Ltd.	https://lifesciences.tecan.com/software
Wave, Version 2.6.0	Agilent Technologies	https://www.agilent.com/en/products/cell-analysis
Biorender	Biorender	https://www.Biorender.com
Other		
Seahorse XF, 24 well, 96 well	Agilent Technologies	XFe24, Cat#102342-100; XFe96, Cat#103793-100
Seahorse XF Tech note 2016	Agilent Technologies	5991-7145EN
SwissProt FASTA database, (Mus musculus (TaxID=10900, version 2022-01)	SwissProt	https://www.uniprot.org/proteomes/

Continued

REAGENT or RESOURCE	SOURCE	IDENTIFIER
Ultimate 3000 liquid chromatography system coupled with the EASY spray ion source and Orbitrap Fusion Lumos tribrid mass spectrometer	Thermofisher Scientific	https://www.thermofisher.com
Glucometer Contour	Bayer AG	https://www.bayer.com/de/
Tecan reader Infinite 200	Tecan Group Ltd.	https://www.tecan.de/
Whole Body Composition Analyzer The EchoMRI™-100H	Echo MRI	http://www.echomri.com/Body_Composition_Mice_2MHz.aspx
PhenoMaster	TSE Systems	https://www.tse-systems.com/
Gas Chromatography System 6890N	Agilent Technologies	https://www.agilent.com/
Fused Silica Capillary Column FS-FFAB-CB-0.25	CS - Chromatographie Service GmbH	https://www.cs-chromatographie.de/
Bioruptor® Bioruptor® Pico	Diagenode SA	https://www.diagenode.com/
NGS Sequencer	Illumina	NextSeq550™
Laboratory animals diet	ssniff Spezialdiäten GmbH	Rat/Mouse extrudate; 58% carbohydrate, 9% fat, 33% protein

RESOURCE AVAILABILITY

Lead contact

Further information and requests for resources and reagents should be directed to and will be fulfilled by the lead contact: Birgit Knebel (birgit.knebel@ddz.de).

Materials availability

This study did not generate new unique reagents.

Data and code availability

Mass spectrometry data have been deposited at the ProteomeXchange Consortium via the PRIDE partner repository and are publicly available as of the date of publication. Accession number is listed in the key resources table. Transcriptome and Methylome data have been deposited at NCBI GEO and are publicly available as of the date of publication. Accession numbers are listed in the key resources table. This paper does not report original code. Any additional information required to reanalyze the data reported in this paper is available from the lead contact upon request.

EXPERIMENTAL MODEL AND STUDY PARTICIPANT DETAILS

Male C57BL/6 mice (RRID:MGI:7264769) (12 weeks old) were kept (5-6 animals per cage) under standard laboratory conditions (12h light/12h dark cycle, 22-24°C, *ad libitum* access to tap water and standard chow diet. All experiments were approved (LANUV, NRW, Germany (81-02.04.2017.A421) and performed according to German law on animal protection and the 'Principle of Laboratory animal care' (NIH-Publikation Nr. 85-23, revised 1996). The animals were exposed to our established chronic variable stress (Cvs) protocol.[27,76] In brief, animals were exposed to 2 stressors per day in alternating order for a period of 15 days: single cage housing (i) on a shaker (100 rpm, 1h), (ii) with cold exposure without bedding (4°C, 1h), (iii) overnight in an oversized cage, (iv) 30 min restraint, (v) warm water swim (30°C, 20 min). The unstressed control (Ctrl) group was handled with special care. Four experimental cohorts were used: 1. for indirect calorimetry and acute analyses in primary hepatocytes (n=5 animals per group); 2. for body composition and liver tissue data including acute proteome, methylome and transcriptome (acuteCVS; acuteCtrl) (n=6 animals per group); 3. for methylation and transcriptional analyses after a 3-month recovery phase (recoveryCvs; recoveryCtrl) (n=3-5 animals per group); 4. for analyses in primary hepatocytes after the recovery phase (n=5 animals per group).

At age of 15 weeks (acute) or 27 weeks (recovery), mice were sacrificed by CO_2 asphyxiation. Primary hepatocytes were isolated by two-step perfusion protocol as described,[11] and serum-starved overnight prior to experimental procedures. Liver biopsies were immediately used for cell fractioning (600xg, 11,000xg fraction) according to our established protocol.[38] In brief, 200 mg liver tissue was homogenized in 1 ml isolation buffer (70 mM sucrose, 210 mM mannitol, 5 mM HEPES/KOH, 1 mM EGTA, pH 7.2) and centrifuged (600xg, 20 min, 4°C) for 600xg fraction. Supernatant was centrifuged (11,000xg, 20 min, 4°C) and the pellet was resuspended in 200 μl isolation buffer for 11.000xg fraction. Remaining biopsy material was snap frozen at -80°C.

In vivo analyses

Glucose tolerance test (GTT) was performed by intraperitoneal injection of mice with glucose (2 g/kg body weight) after 6h fasting. Pyruvate tolerance test (PTT) was performed by intraperitoneal injection of pyruvate solution (1.5 g pyruvate/kg body weight) after 16h fasting. Blood glucose was monitored (0, 15, 30, 60, 120 min) after glucose or pyruvate injection.[27] Body composition was analysed with nuclear magnetic resonance (NMR) (n=6 animals per group) as previously described.[38]

Total energy expenditure (EE) and respiratory exchange ratio (RER) were measured at 22°C using metabolic cages (n=5 animals/group) according to manufacturer's recommendations (TSE Systems, Bad Homburg, Germany) with unrestricted access to food and water as described.[38] In brief, after 24h acclimatization, measurements were taken every 30 min for two complete circadian cycles (48h) starting with the light phase. Total energy expenditure (EE), respiratory exchange ratio (RER), fatty acid oxidation (FAO) and carbohydrate oxidation (CHO) were calculated as described.[33,38]

Plasma analyses

Blood samples were collected by cardiac puncture after CO_2 asphyxiation. Glucose, lactate, glutamate, triglyceride levels (Sigma-Aldrich/ MERCK, Darmstadt, Germany), leptin, glucagon and insulin (Bio-Plex Pro™, Bio-Rad, Munich, Germany) were determined. Non-esterified fatty acid (NEFA) content was determined by a gas chromatography system as described.[77]

Ex vivo analyses in primary hepatocytes

De novo lipogenesis (DNL) was quantified by ^{14}C-acetate incorporation. FAO was quantified by $^{14}CO_2$ release from ^{14}C-palmitate oxidation normalized to protein content. Gluconeogenesis activity was quantified by glucose secretion after pyruvate/lactate stimulation. Energy phenotype was assessed using measures of glycolytic activity in response to glucose administration as extracellular acidification rate (ECAR) against oxidative activity in form of oxygen consumption rate (OCR) measures of untreated (basal) and FCCP-treated (uncoupled) primary hepatocytes. All procedures were performed as described.[11]

Ex vivo analyses in liver tissue

Liver biospies were processed according to the respective assay protocol for determination of ß-hydroxybutyrate, glucose, triglyceride levels and reactive oxygen (ROS) species. Citrate synthase (CS) activity, cytochrome-c-oxidase activity, NAD^+, NADH, and FAD^+ level were assessed in the 11,000xg fraction. All procedures were performed as described.[11] Global Methyltransferase and SIRT activity (SIRTs; histone deacetylases class III; (SIRT1, SIRT2, SIRT3, SIRT4, SIRT5, SIRT6, SIRT7) was analysed using 1μg of the lysed 600 xg fraction.[27]

Mitochondrial copy number was determined by the relative amount of mitochondrial DNA (mtDNA) to nuclear DNA (nDNA) by qPCR (n=5 animals per group) as described[78] and using mtDNA sequence without homology to nuclear DNA.[74]

Hepatic mitochondrial respiratory function was assessed using extracellular flux analyses (Seahorse XF, Agilent, Taufkirchen, Germany) as described.[11,38] 5 μg of enriched liver mitochondria from freshly isolated 11,000xg fraction were used per single reaction/well. Electron flow and coupling experiments were performed as described in the manufacturer's application note (Agilent Technologies, Inc., 2016, 5991-7145EN) with substrate and compound/inhibitor concentrations previously described.[11] All OCR measurements were performed in technical triplicates for each animal (n=6 per group) with equal protein amount of 11,000xg fraction per well. Mitochondrial content marker CS activity was used for normalization.[28,29]

Proteome analyses

Differences in protein composition of the 11,000xg fraction were analysed in 5 animals per group using a label-free proteomic analysis method by LC-MS/MS, as described.[11,38] Briefly, MS data were acquired using data-dependent (DDA) and data-independent (DIA, 38 windows) MS/ MS scanning methods. Proteomic data were further analysed by Spectronaut® v.17 (Biognosis, Schlieren, Switzerland). Analyses details are given in Table S1. Data were analysed for Z-score significance for each condition in relation to the experimental mean.

Transcriptome analyses

For transcriptome analyses, total RNA was extracted with standard procedures from snap-frozen liver biopsies (Qiagen, Hilden, Germany). Genome-wide expression analysis (n=5 samples per condition) was performed using Mouse Gene (MTA) arrays (Thermo Fisher Scientific, Darmstadt, Germany) as described starting from 150 ng total RNA.[11] Gene expression data were further analysed with Transcriptome Analysis Console™ v.4.01 (Thermo Fisher, Darmstadt, Germany), and knowledge-based transcriptome analyses were performed using IPA® (QIAGEN Inc., https://digitalinsights.qiagen.com/IPA, Spring release 2023),[79] with set thresholds to ≥1.5-fold differences, p-value < 0.05.

Methylome analyses

Genomic DNA was extracted from 10 mg frozen liver tissue (n=3-5 animals per condition). To enrich DNA fragments harboring methylated cytosines (^{met}C), methylated DNA immunoprecipitation, (MeDIP) was performed with an antibody directed to ^{met}C (EpiXplore™ Methylated DNA Enrichment Kit (Takara Bio Europe, Saint-Germain-en-Lage, France). NGS sequencing libraries were constructed from ^{met}C immuno-precipitated DNA fragments, and paired-end sequenced. Analyses details are given in Table S2.

Enrichment analyses based on edgeR log fold change and edgeR p-value were performed with Gene ontology (GO) enrichment analyses using Panther[80] and knowledge-based with IPA®.[79] R packages Circus plot[81] was used for visualization of omics data. Further experimental details are given in Table S2.

QUANTIFICATION AND STATISTICAL ANALYSIS

Non-omics data are reported as mean with 95% confidence interval (CI) unless otherwise stated for the specified number of animals. For two variables the Mann-Whitney test and for more than two groups a two-way analysis of variance (ANOVA) with Tukey was performed. Correlation analyses were performed using linear regression calculations and verified by Pearson Correlation ($p < 0.05$). Estimation plots were calculated based on the Z-Score data by unpaired t-test and 95% CI ($p < 0.05$). GraphPad Prism 9.5.0 software (GraphPad Software Inc., La Jolla, USA) was used to perform all statistical analyses.